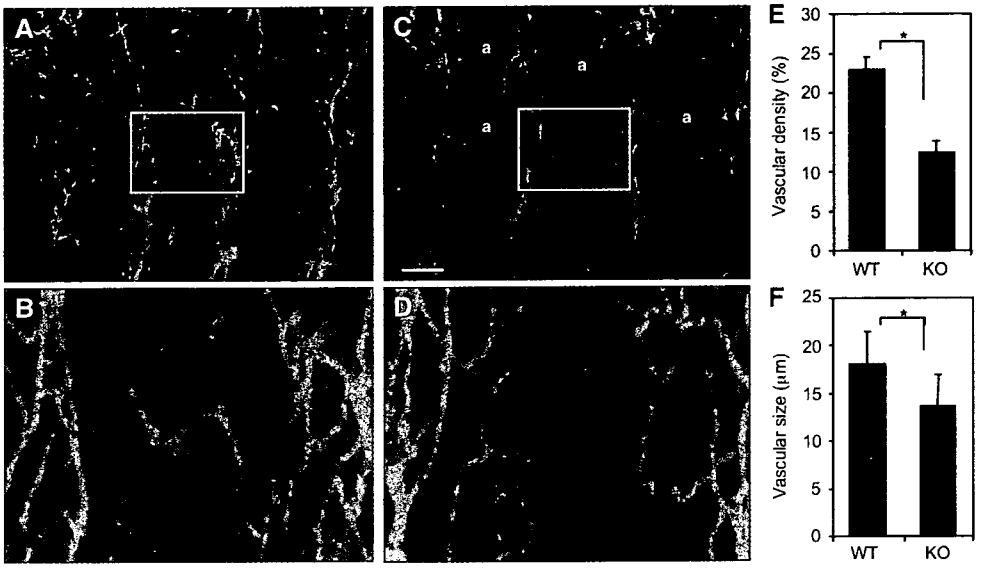

Figure 8 Lectin staining of tracheal blood vessels. (A–D) Comparison of tracheal blood vessels in 8-week-old WT (**A**, **B**) and apelin-deficient (**C**, **D**) mice stained by intravenous injection of fluorescein-labelled lectin. a in (C) means avascular area. (B) and (D) show a high-power view of the area indicated by the box in (A) and (C), respectively. Scale bar in (C) indicates 200 μm (A, C) and 60 μm (B, D). (**E**) Quantitative evaluation of vascular density from apelin-deficient (KO) versus WT mice. $^*P<0.001$. Vascular density from 10 random fields was counted. (**F**) Quantitative evaluation of vascular size of blood vessels in the trachea from apelin-deficient (KO) versus WT mice. Vascular size was measured as the length between two parallel red lines as indicated in (B) and (D). $^*P<0.001$ (100 vessels from 3 mice were examined).

Role of apelin in Ang1-induced enlargement of capillary size

We isolated apelin from ECs under the activation of Tie2 by Angl. Next, using apelin-deficient mice, we observed whether Angl-induced enlargement of blood vessels is suppressed in the absence of apelin. In this experiment, we mated apelin-deficient mice with Angl Tg mice and observed the caliber size of the capillaries in the dermis (Figure 9).

In apelin-deficient mice, the caliber size of the capillary in the dermis was narrower compared with that in WT mice (Figure 9A and B and Supplementary Figure 11). We confirmed that CD31-positive cells are from blood vessels but not from lymphatic vessels, by double staining with LYVE1, a specific marker for lymphatic ECs (Supplementary Figure 11). As previously reported (Suri *et al*, 1998), Angl Tg mice showed enlarged capillary formation in the dermis, but this effect of Angl was abolished by the lack of apelin (Figure 9A and B). However, apelin deficiency did not completely suppress Angl-induced enlargement of blood vessels, suggesting that other molecules upregulated by Tie2 activation might be involved in the caliber size determination of capillaries *in vivo*. On the other hand, the generation of extremely enlarged blood vessels, with a caliber size of more than $10^4\,\mu m^2$, observed in Angl Tg mice, was completely suppressed in the absence of apelin (Figure 9A and C). Therefore, we concluded that one of the molecules affected by Angl for enlargement of the capillary was apelin in ECs.

Apelin induces an enlarged endothelial sheet in P-Sp culture system

In vivo analysis suggested that apelin regulates the caliber change of blood vessels. Next, we observed blood vessel formation by using *in vitro* (P-Sp) organ culture system, which has previously been shown to mimic *in vivo* vasculogenesis and angiogenesis (Takakura *et al*, 1998, 2000). P-Sp explants from mice at E9.5 contain early developed DA. In the P-Sp culture system, ECs show two different morphologies. One is a sheet-like structure (vascular bed) that develops in the early stages of the culture. The other is a network-like structure, constructed from the ECs sprouting from the vascular bed. Previously, we identified that the sheet-like formation mimics vasculogenesis and the network formation mimics angiogenesis, which is a process of capillary sprouting from pre-existing vessels (Takakura *et al*, 2000). Therefore, as apelin-mutant embryos showed narrow ISVs, which were sprouted from the DA, this suggests that the P-Sp culture system can reproduce the *in vivo* effects of apelin.

In the P-Sp culture system, OP9 stromal cells were used as feeder cells for P-Sp explants. We induced apelin expression on OP9 cells (Figure 3B) and observed the effect. Compared to the control culture (Figure 10Aab), network-forming ECs became thick and the vascular density of the network area was high (Figure 10Acd), although the amount of branching was the same. By contrast, the suppression of apelin/APJ function, by blocking antibody against apelin, induced thin network formation by ECs (Figure 10Aef). When the network-forming area of ECs was evaluated, it was higher in apelin-expressing OP9 cells (OP9/apelin) than in control OP9 cells (OP9/vector); this effect by apelin was completely blocked by anti-apelin mAb (Figure 10Ag).

In the P-Sp culture system, we found that APJ is expressed in the network-forming ECs sprouted from the vascular bed as observed in the ISVs, but not in the ECs forming the sheet (Figure 10B). *In vitro* analysis indicated that the apelin/APJ system might affect cell-to-cell aggregation or assembly, and therefore we stained network-forming ECs by anti-VE-cadherin antibody. As observed in Figure 10C, apelin enhanced the assembly of ECs. Interestingly, in the control P-Sp culture, the network-forming endothelial layer, composed of one or two ECs, migrated in a peripheral direction along with the ECs at the tip (Figure 10Cab). On the other hand, when apelin was overexpressed on OP9 cells, many aggregated

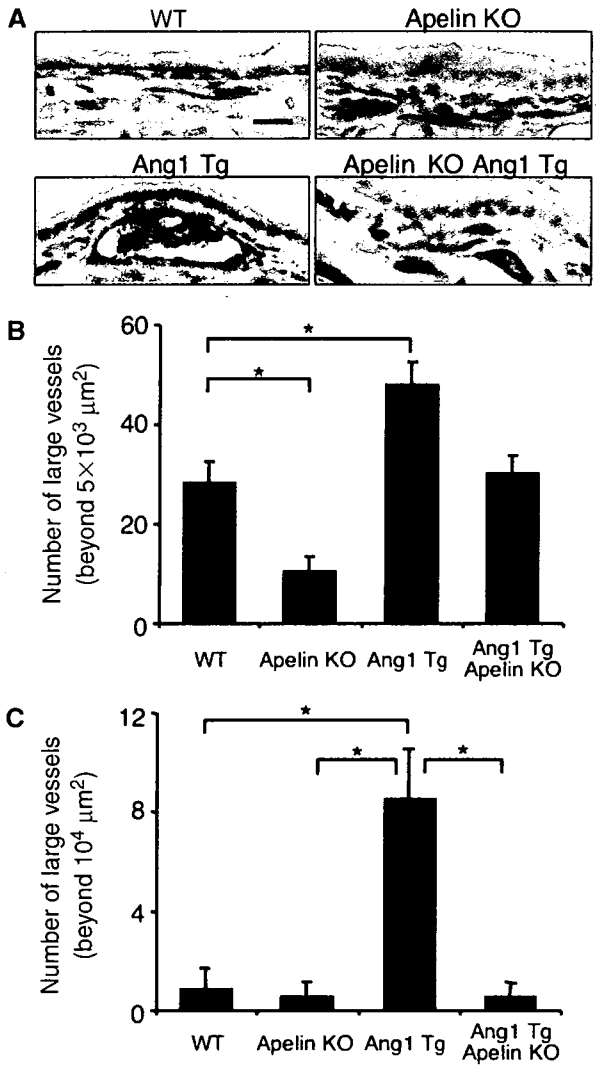

Figure 9 Apelin/APJ system is involved in Angl-induced vascular enlargement. (**A**) Sections of ear skin stained with anti-CD31 mAb. Ear skin was prepared from 8-week-old WT, apelin-deficient (apelin KO), Angl Tg mice, or apelin-deficient mice mated with Angl Tg mice (apelin KO/Angl Tg). Scale bar indicates 30 μm. (**B**, **C**) Quantitative evaluation of the number of enlarged blood vessels composed of a luminal cavity of more than 5000 μm^2 (B) or more than 10^4 μm^2 (C) in the skin from mice as described in (A). Thirty random fields were observed from sections of three independent mice as described in (A). $^*P<0.01$.

ECs migrated along with the ECs at the tip (Figure 10Ccd), and this effect was completely suppressed by anti-apelin mAb (Figure 10Cef). These results indicated that apelin induces an enlarged endothelial sheet when angiogenesis is taking place.

Discussion

The knowledge of how vascular cells commit from their progenitor cells and generate a closed cardiovascular circulatory system has accumulated in recent years, mostly by the isolation and functional analysis of molecules associated with blood vessel formation. However, little is known regarding the molecular events that regulate EC morphogenesis, especially the caliber size determination of blood vessels. Data documented here, from both *in vitro* and *in vivo* analysis, showed that apelin regulates the enlargement of newly developed blood vessels during angiogenesis.

In angiogenesis, how blood vessels 'decide' their appropriate size is very important to the organization of the adjustment of tissue and organ demand for oxygen and nutrients. Our analysis clearly showed that APJ expression was induced by VEGF, which, in turn, is well known to be induced by tissue hypoxia (Liu *et al*, 1995). This indicates that, under tissue hypoxia, blood vessels have an opportunity to enlarge their size and the reduction of APJ expression finalizes the enlargement of blood vessel caliber under tissue normoxia. Indeed, in the retina, APJ was observed temporally in the radial vessels and the associated capillaries of retina from day 3 to day 12 after birth, but APJ expression on ECs was attenuated in the later stage (Saint-Geniez *et al*, 2002). As reported in the retina, we also found that APJ expression was observed in ECs sprouted from the DA and ECs on blood vessels in the neonatal dermis of mice (data not shown), but that it gradually disappeared with maturity. These expression patterns strongly suggested that APJ plays a spatio-temporal role in the maturation of blood vessels by transient expression on ECs of blood vessels where angiogenesis is taking place. Therefore, we concluded that one of the molecules associated with the regulation of blood vessel diameter was apelin in the ECs.

Based on our results presented here, it appears that VEGF, Angl and apelin regulate caliber size in a concerted fashion, as follows. Upon stimulation by VEGF, ECs sprouted from pre-existing vessels may express APJ. Subsequently, Angl stimulates these sprouted ECs to induce apelin expression. In the presence of both VEGF and apelin, the ECs start to proliferate, adhere and form contacts with each other through junctional proteins, and construct enlarged blood vessels. Apelin has been reported to induce angiogenesis in the Matrigel plug assay (Kasai *et al*, 2004) and also chemotaxis (Cox *et al*, 2006). In our experiments using the Matrigel plug assay, we found that apelin induced migration, rather than proliferation, of ECs (Supplementary Figure 14). Moreover, we confirmed that like VEGF, apelin modified the cytoskeleton structure (Supplementary Figure 15). Therefore, apelin may induce mobilization of ECs in the process of EC-to-EC assembly.

As we found, apelin deficiency suppressed the enlargement of ISVs during early embryogenesis. Furthermore, it has been reported elsewhere that Angl and VEGF are expressed in intersomitic or somitic tissues (Davis *et al*, 1996; Lawson *et al*, 2002) and that apelin is coexpressed with APJ-positive ECs in ISVs. Indeed both Tie2 and Angl mutant embryos showed impaired ISV formation (Dumont *et al*, 1994; Sato *et al*, 1995). Therefore, it appears that these three components may be involved in the regulation of caliber size change of the ISVs.

Transgenic overexpression of Angl in the keratinocyte induced enlarged blood vessels in the dermis (Suri *et al*, 1998) and administration of a potent Angl variant was also reported to induce enlargement of blood vessels (Cho *et al*, 2005; Thurston *et al*, 2005). Therefore, Angl expression may be a key determinant of caliber size during angiogenesis. Angl is usually produced from MCs in cells composing blood vessels (Davis *et al*, 1996), However, we previously reported that hematopoietic stem cells (HSCs) producing Angl migrate into avascular areas before the ECs start to migrate, and that this Angl from HSCs induces angiogenesis by promoting the chemotaxis of ECs (Takakura *et al*, 2000). Moreover, recently,

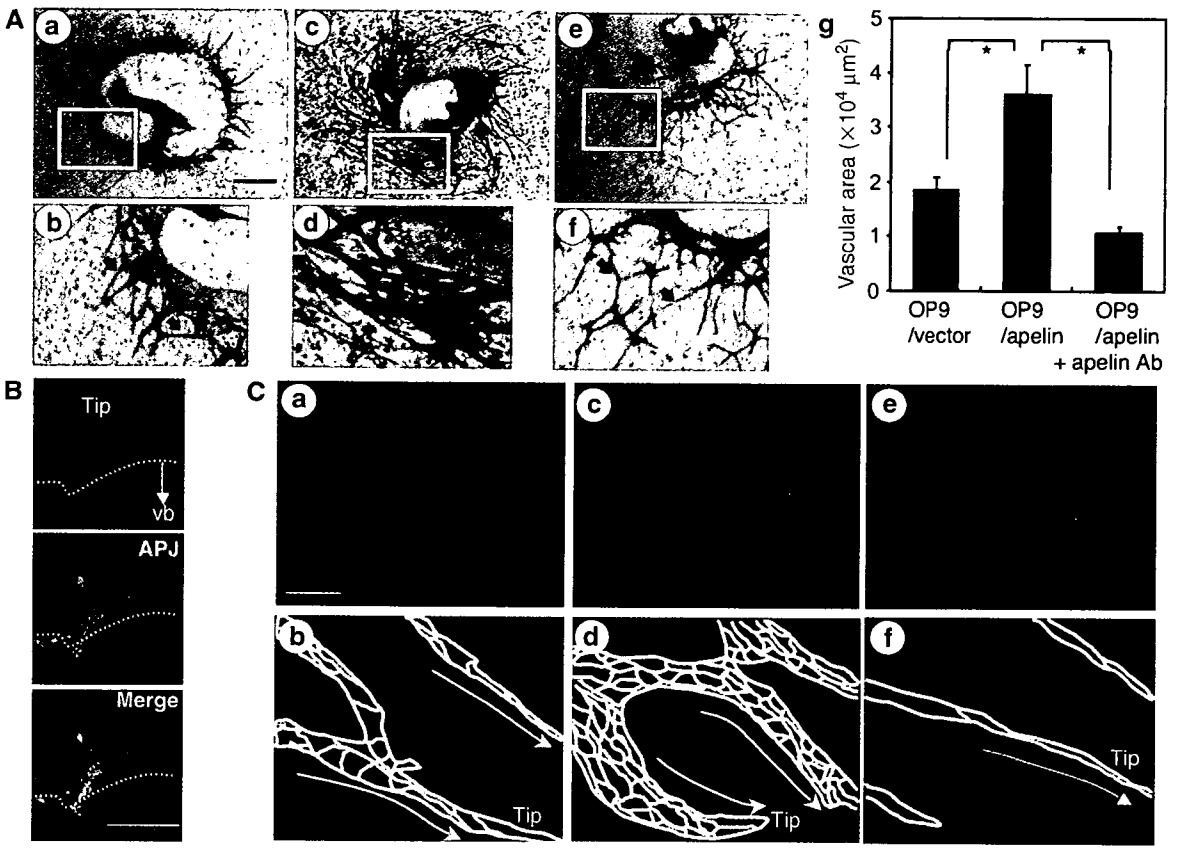

Figure 10 Effect of apelin on the P-Sp culture system. (**A**) Effect of apelin on the network-like structure of ECs in the P-Sp culture system. P-Sp explants from E9.5 mouse embryos were cultured for 7 days on OP9/vector (a, b) or OP9/apelin, in the presence of B220 control mAbs (c, d) or anti-apelin mAbs (e, f), and then stained with anti-CD31 mAb. (b), (d) and (f) are higher magnifications of areas indicated by the box in (a), (c) and (e), respectively. Arrows indicate network-forming ECs. Scale bar indicates 1 mm (a, c, e) or 200 μm (b, d, f). (g) Quantitative evaluation of the vascular network area cultured as above. Endothelial space per 500 μm length of network-forming ECs was measured in 10 random fields. $^*P<0.001$. (**B**) Expression of APJ in ECs of P-Sp culture. Cells on culture plates were stained with anti-CD31 (red) and anti-APJ (green) antibodies. Tip, tip EC. Dotted line indicates the border of the vascular bed (vb). Note APJ expressed on ECs forming a network-like structure. Scale bar indicates 100 μm. (**C**) Network-forming ECs derived from P-Sp explants cultured on OP9/vector (a, b), OP9/apelin in the presence of control B220 mAbs (c, d) or OP9/apelin in the presence of anti-apelin mAbs (e, f) for 7 days were stained with anti-VE-cadherin (red) mAbs. Scale bar indicates 20 μm. Because nuclear staining cannot distinguish the nuclei of ECs from those of OP9 cells, only VE-cadherin expression was revealed. Therefore, the EC-to-EC boundary expressed by VE-cadherin is presented (b, d, f). Tip, tip EC. Migration direction of tip EC is indicated by the arrow.

we found that HSCs induce enlargement of blood vessels observed in the fibrous cap surrounding tumors (Okamoto *et al*, 2005) and Ang1 from HSCs in embryos, as well as adults, induces structural stability of newly developed blood vessels as a physiological function during angiogenesis (Yamada and Takakura, 2006). Therefore, it is possible that Ang1 from the HSC population, which are frequently observed in ischemic regions, is the one source of Tie2 activation and results in the production of apelin from ECs.

It has been suggested that apelin mediates phosphorylation and activation of endothelial NO synthase in ECs, causing NO release from ECs (Tatemoto *et al*, 2001; Ishida *et al*, 2004). NO is well known to induce relaxation of MCs, resulting in dilation of blood vessels. Therefore, it is possible that apelin causes endothelium-dependent vasodilatation by triggering the release of NO from ECs. In our analysis, however, we observed that apelin induced enlarged cord formation of HUVECs on Matrigel, and enlarged spheroids of HUVECs in the liquid culture. These culture conditions do not contain MCs, which indicates that apelin can induce enlargement of blood vessels without affecting MCs.

Knockout studies of the apelin gene suggested that molecular cues other than apelin rescue the narrow caliber size of blood vessels by compensational upregulation, because in the early stage of embryogenesis the narrow caliber of ISVs, observed in apelin-mutant embryos, was rescued in the later stage (data not shown). As observed in apelin knockout mice, APJ mutant mice appeared healthy as adults (Ishida *et al*, 2004); however, the requisite role of the apelin/APJ system in blood vessel formation was reported in *Xenopus* (Cox *et al*, 2006; Inui *et al*, 2006). The reason of this discrepancy is not known, but functionally redundant ligand/receptor or signalling pathways may be present in mice.

Tube formation is a fundamental mechanism for organ and tissue generation in most major organs, such as lung and kidney, as well as the vasculature. The molecular mechanism involved in tube generation is not clearly understood. During angiogenesis, neovessels must be generated by both single cell hollowing and cord hollowing methods. Through the analysis of the precise functional relationship between the molecules described above including the apelin/APJ system, anatomically described diverse tube formation of the vasculature will be further clarified at the molecular level.

Materials and methods

Animals

C57BL/6 mice and ICR mice were purchased from Japan SLC (Shizuoka, Japan) at 8 weeks of age and used between 8 and 12 weeks of age. Ang1Tg mice (Suri *et al*, 1998) with a C57BL/6 background were provided by Dr GD Yanchopoulos (Regeneron Pharmaceuticals Inc., Tarrytown, NY). Animal care in our laboratory was in accordance with the guidelines of Kanazawa and Osaka University for animal and recombinant DNA experiments.

Plasmids and transfection

The mouse *Apelin* gene was cloned into the pCAGSIH expression vector. Lipofectamine Plus reagent (Invitrogen Life Technologies, Carlsbad, CA) was used to transfect cells with this plasmid and clones of cells exhibiting stable transfection were obtained by antibiotic resistance selection using G418 (Gibco, Grand Island, NY). Primer pairs for PCR to detect transfected gene are listed in Supplementary Table S1.

Tissue preparation, immunohistochemistry and flow cytometry

Tissue fixation, preparation of tissue sections and staining of sections or cultured cells with antibodies were performed as described previously (Takakura *et al*, 2000). An biotin-conjugated anti-CD31 mAb (Pharmingen, San Diego, CA), anti-apelin Ab (4G5; Kawamata *et al*, 2001) and anti-APJ polyclonal Ab were used in the staining of tissue sections or cultured cells. To obtain a specific antibody against mouse APJ, a rabbit was immunized with a synthetic peptide (CHEKSIPYSQETLVD) derived from the C-terminal region of APJ. Antisera were affinity purified with the same peptide. Preimmunized rabbit immunoglobulins were used as a negative control to confirm specific staining. Sections were counterstained with hematoxylin or propidium iodide. The sections were observed using an Olympus IX-70 microscope (Olympus, Tokyo, Japan) and images were acquired with a CoolSnap digital camera (Roper Scientific, Trenton, NJ). Whole-mount immunohistochemistry using anti-CD31 mAb or anti-APJ was performed as previously described (Takakura *et al*, 1998). Stained embryos were observed under a Leica MZ16FA stereomicroscope (Leica, Solms, Germany) and photographed with a DC120 digital camera (Pixera, Los Gatos, CA). In all assays, we used an isotype-matched control Ig as a negative control and confirmed that the positive signals were not derived from nonspecific background. Investigation of the density and morphology of microvessels in lectin-stained whole mount of tracheal blood vessels was performed as described (Yamada and Takakura, 2006). In brief, after anaesthesia with sodium pentobarbital, mice were injected into the tail vein with fluorescein-labelled *Lycopersicon esculentum* lectin (Vector Laboratories, Burlingame, CA), which binds uniformly to the luminal surface of ECs and adherent leukocytes. Lectin-stained tracheas were removed from apelin-deficient and WT mice and analysed under a fluorescence microscope. Images were processed using Adobe Photoshop 6.0 software (Adobe Systems, San Jose, CA). Flow cytometric analysis was performed as previously described (Yamada and Takakura, 2006). FITC-conjugated anti-CD45 mAb and PE-conjugated anti-CD31 mAb (Pharmingen) were used. The stained cells were analysed by FACS Calibur (Becton Dickinson, Franklin Lakes, NJ) and sorted by EPICS flow cytometer (ALTRA; Beckman Coulter, Fullerton, CA).

Cell culture

4×10^6 HUVECs were cultured in six-well plates for 12 h in Humedia EG2 (Kurabo, Osaka, Japan). Cells were then incubated in M199 medium supplemented with 1% fetal bovine serum (FBS). After 3 h of serum deprivation, cells were incubated with basal medium containing 500 ng/ml of Ang1 (R&D Systems, Minneapolis, MN), 100 ng/ml of apelin (Bachem, Bubendorf, Switzerland) or 20 ng/ml of VEGF-A_{165} (PeproTech, Rocky Hill, NJ).

The culture of P-Sp explant was performed as previously reported (Takakura *et al*, 2000). OP9 cells stably transfected with a pCAGSIH expression vector carrying the cDNA for mouse apelin or mock vector were used as feeder cells (OP9/apelin or OP9/vector, respectively) in the presence or absence of anti-apelin monoclonal blocking antibody (4G5; see Supplementary Figure 16 for functional analysis of this antibody in the inhibition of the apelin/APJ system) or control anti-B220 mAb. After 7 days of culture, the cultured cells on OP9 cells were fixed and stained with mAbs. For the culture of dissociated ECs from the AGM region, the regions were excised from E11.5 ICR embryos and dissociated by dispase II (Boehringer Mannheim, Mannheim, Germany) as previously described (Yamada and Takakura, 2006). Cells were suspended in DMEM supplemented with 15% fetal calf serum and cultured in OP9/vector or OP9/apelin seeded on 24-well plates in the presence of murine SCF (100 ng/ml; PeproTech), bFGF (1 ng/ml; R&D Systems) and OSM (10 ng/ml; R&D Systems). To this culture, we added 10 μg/ml anti-apelin or anti-B220 mAb. After 6 days of culture, the cells were fixed and double stained with anti-CD31 mAb and anti-VE-cadherin mAb (BD Pharmingen, San Jose, CA), or anti-CD31 mAb and claudin5 mAb (Abcam Inc., Cambridge, MA). Stained samples were analysed by confocal laser scanning microscopy (LSM510, Carl Zeiss, Germany). For the evaluation of apelin in promoting proliferation of HUVECs, HUVECs were cultured for 24 h in medium plus growth supplements and then for an additional 48 h in medium with or without apelin (10–100 ng/ml), VEGF (10 ng/ml) or apelin plus VEGF. Cell proliferation was then evaluated by directly counting the cell number.

Aortic ring culture for angiogenesis assay

Descending thoracic aortas were isolated from apelin-deficient mice. Under a stereomicroscope, multiple 1-mm-thick aortic rings were prepared. Rings were then placed between two layers of type I collagen gel (Cellmatrix Type IA, Nitta Zeratin, Osaka, Japan), supplemented with Medium 199, 20% FBS in the presence or absence of VEGF (20 ng/ml) or apelin (200 ng/ml). The cultures were kept at 37°C in a humidified environment for a week and examined every second day under an Olympus microscope (IX70).

Statistical analysis

All data are presented as mean±standard deviation (s.d.). For statistical analysis, the statcel2 software package (OMS) was used with analysis of variance performed on all data followed by Tukey–Kramer multiple comparison test. When only two groups were compared, two-sided Student's *t*-test was used.

Supplementary data

Supplementary data are available at *The EMBO Journal* Online (http://www.embojournal.org).

Acknowledgements

We thank Dr GD Yanchopoulos (Regeneron Pharmaceuticals Inc.) and Dr Y Oike (Keio University, Tokyo, Japan) for providing us with Ang1Tg mice and with anti-LYVE-1 antibody, respectively. Moreover, we thank N Fujimoto for preparation of plasmid DNA and K Fukuhara for administrative assistance. This work was partly supported by a Grant-in-Aid from The Ministry of Education, Culture, Sports, Science and Technology of Japan to NT.

References

Adams RH, Wilkinson GA, Weiss C, Diella F, Gale NW, Deutsch U, Risau W, Klein R (1999) Roles of ephrinB ligands and EphB receptors in cardiovascular development: demarcation of arterial/venous domains, vascular morphogenesis, and sprouting angiogenesis. *Genes Dev* **13:** 295–306

Ashley EA, Powers J, Chen M, Kundu R, Finsterbach T, Caffarelli A, Deng A, Eichhorn J, Mahajan R, Agrawal R, Greve J, Robbins R, Patterson AJ, Bernstein D, Quertermous T (2005) The endogenous peptide apelin potently improves cardiac contractility and reduces cardiac loading *in vivo*. *Cardiovasc Res* **65:** 73–82

Carmeliet P (2003) Angiogenesis in health and disease. *Nat Med* **9:** 653–660

Cho CH, Kim KE, Byun J, Jang HS, Kim DK, Baluk P, Baffert F, Lee GM, Mochizuki N, Kim J, Jeon BH, McDonald DM, Koh GY

(2005) Long-term and sustained COMP-Ang1 induces long-lasting vascular enlargement and enhanced blood flow. *Circ Res* **97:** 86–94

Cox CM, D'Agostino SL, Miller MK, Heimark RL, Krieg PA (2006) Apelin, the ligand for the endothelial G-protein-coupled receptor, APJ, is a potent angiogenic factor required for normal vascular development of the frog embryo. *Dev Biol* **296:** 177–189

Croitoru-Lamoury J, Guillemin GJ, Boussin FD, Mognetti B, Gigout LI, Cheret A, Vaslin B, Le Grand R, Brew BJ, Dormont D (2003) Expression of chemokines and their receptors in human and simian astrocytes: evidence for a central role of TNF alpha and IFN gamma in CXCR4 and CCR5 modulation. *Glia* **41:** 354–370

Davis S, Aldrich TH, Jones PF, Acheson A, Compton DL, Jain V, Ryan TE, Bruno J, Radziejewski C, Maisonpierre PC, Yancopoulos GD (1996) Isolation of angiopoietin-1, a ligand for the TIE2 receptor, by secretion-trap expression cloning. *Cell* **87:** 1161–1169

De Mota N, Reaux-Le Goazigo A, El Messari S, Chartrel N, Roesch D, Dujardin C, Kordon C, Vaudry H, Moos F, Llorens-Cortes C (2004) Apelin, a potent diuretic neuropeptide counteracting vasopressin actions through inhibition of vasopressin neuron activity and vasopressin release. *Proc Natl Acad Sci USA* **101:** 10464–10469

Devic E, Paquereau L, Vernier P, Knibiehler B, Audigier Y (1996) Expression of a new G protein-coupled receptor X-msr is associated with an endothelial lineage in *Xenopus laevis*. *Mech Dev* **59:** 129–140

Devic E, Rizzoti K, Bodin S, Knibiehler B, Audigier Y (1999) Amino acid sequence and embryonic expression of msr/apj, the mouse homolog of *Xenopus* X-msr and human APJ. *Mech Dev* **84:** 199–203

Dumont DJ, Gradwohl G, Fong GH, Puri MC, Gerstenstein M, Auerbach A, Breitman ML (1994) Dominant-negative and targeted null mutations in the endothelial receptor tyrosine kinase, tek, reveal a critical role in vasculogenesis of the embryo. *Genes Dev* **8:** 1897–1909

Edinger AL, Hoffman TL, Sharron M, Lee B, Yi Y, Choe W, Kolson DL, Mitrovic B, Zhou Y, Faulds D, Collman RG, Hesselgesser J, Horuk R, Doms RW (1998) An orphan seven-transmembrane domain receptor expressed widely in the brain functions as a coreceptor for human immunodeficiency virus type 1 and simian immunodeficiency virus. *J Virol* **72:** 7934–7940

Ferrara N, Alitalo K (1999) Clinical applications of angiogenic growth factors and their inhibitors. *Nat Med* **5:** 1359–1364

Ferrara N, Gerber HP, LeCouter J (2003) The biology of VEGF and its receptors. *Nat Med* **9:** 669–676

Gale NW, Yancopoulos GD (1999) Growth factors acting via endothelial cell-specific receptor tyrosine kinases: VEGFs, angiopoietins, and ephrins in vascular development. *Genes Dev* **13:** 1055–1066

Gerhardt H, Betsholtz C (2003) Endothelial-pericyte interactions in angiogenesis. *Cell Tissue Res* **314:** 15–23

Inui M, Fukui A, Ito Y, Asashima M (2006) Xapelin and Xmsr are required for cardiovascular development in *Xenopus laevis*. *Dev Biol* **298:** 188–200

Ishida J, Hashimoto T, Hashimoto Y, Nishiwaki S, Iguchi T, Harada S, Sugaya T, Matsuzaki H, Yamamoto R, Shiota N, Okunishi H, Kihara M, Umemura S, Sugiyama F, Yagami K, Kasuya Y, Mochizuki N, Fukamizu A (2004) Regulatory roles for APJ, a seven-transmembrane receptor related to angiotensin-type 1 receptor in blood pressure *in vivo*. *J Biol Chem* **279:** 26274–26279

Jain RK (2005) Normalization of tumor vasculature: an emerging concept in antiangiogenic therapy. *Science* **307:** 58–62

Kasai A, Shintani N, Oda M, Kakuda M, Hashimoto H, Matsuda T, Hinuma S, Baba A (2004) Apelin is a novel angiogenic factor in retinal endothelial cells. *Biochem Biophys Res Commun* **325:** 395–400

Katugampola SD, Maguire JJ, Matthewson SR, Davenport AP (2001) [(125)I]-(Pyr(1))Apelin-13 is a novel radioligand for localizing the APJ orphan receptor in human and rat tissues with evidence for a vasoconstrictor role in man. *Br J Pharmacol* **132:** 1255–1260

Kawamata Y, Habata Y, Fukusumi S, Hosoya M, Fujii R, Hinuma S, Nishizawa N, Kitada C, Onda H, Nishimura O, Fujino M (2001) Molecular properties of apelin: tissue distribution and receptor binding. *Biochim Biophys Acta* **1538:** 162–171

Kleinz MJ, Davenport AP (2004) Immunocytochemical localization of the endogenous vasoactive peptide apelin to human vascular and endocardial endothelial cells. *Regul Pept* **118:** 119–125

Koller A, Huang A (1999) Development of nitric oxide and prostaglandin mediation of shear stress-induced arteriolar dilation with aging and hypertension. *Hypertension* **34:** 1073–1079

Korff T, Augustin HG (1998) Integration of endothelial cells in multicellular spheroids prevents apoptosis and induces differentiation. *J Cell Biol* **143:** 1341–1352

Lawson ND, Vogel AM, Weinstein BM (2002) sonic hedgehog and vascular endothelial growth factor act upstream of the Notch pathway during arterial endothelial differentiation. *Dev Cell* **3:** 127–136

Lindahl P, Johansson BR, Leveen P, Betsholtz C (1997) Pericyte loss and microaneurysm formation in PDGF-B-deficient mice. *Science* **277:** 242–245

Liu Y, Cox SR, Morita T, Kourembanas S (1995) Hypoxia regulates vascular endothelial growth factor gene expression in endothelial cells. Identification of a 5′ enhancer. *Circ Res* **77:** 638–643

Masri B, Knibiehler B, Audigier Y (2005) Apelin signalling: a promising pathway from cloning to pharmacology. *Cell Signal* **17:** 415–426

O'Dowd BF, Heiber M, Chan A, Heng HH, Tsui LC, Kennedy JL, Shi X, Petronis A, George SR, Nguyen T (1993) A human gene that shows identity with the gene encoding the angiotensin receptor is located on chromosome 11. *Gene* **136:** 355–360

Oettgen P (2001) Transcriptional regulation of vascular development. *Circ Res* **89:** 380–388

Okamoto R, Ueno M, Yamada Y, Takahashi N, Sano H, Suda T, Takakura N (2005) Hematopoietic cells regulate the angiogenic switch during tumorigenesis. *Blood* **105:** 2757–2763

Risau W (1997) Mechanisms of angiogenesis. *Nature* **386:** 671–674

Saint-Geniez M, Masri B, Malecaze F, Knibiehler B, Audigier Y (2002) Expression of the murine msr/apj receptor and its ligand apelin is upregulated during formation of the retinal vessels. *Mech Dev* **110:** 183–186

Sato TN, Tozawa Y, Deutsch U, Wolburg-Buchholz K, Fujiwara Y, Gendron-Maguire M, Gridley T, Wolburg H, Risau W, Qin Y (1995) Distinct roles of the receptor tyrosine kinases Tie-1 and Tie-2 in blood vessel formation. *Nature* **376:** 70–74

Scott IC, Masri B, D'Amico LA, Jin SW, Jungblut B, Wehman AM, Baier H, Audigier Y, Stainier DY (2007) The G protein-coupled receptor agtrl1b regulates early development of myocardial progenitors. *Dev Cell* **12:** 403–413

Simon MC (2004) Vascular morphogenesis and the formation of vascular networks. *Dev Cell* **6:** 479–482

Suri C, Jones PF, Patan S, Bartunkova S, Maisonpierre PC, Davis S, Sato TN, Yancopoulos GD (1996) Requisite role of angiopoietin-1, a ligand for the Tie-2 receptor, during embryonic angiogenesis. *Cell* **87:** 1171–1180

Suri C, McClain J, Thurston G, McDonald DM, Zhou H, Oldmixon EH, Sato TN, Yancopoulos GD (1998) Increased vascularization in mice overexpressing angiopoietin-1. *Science* **282:** 468–471

Szokodi I, Tavi P, Foldes G, Voutilainen-Myllyla S, Ilves M, Tokola H, Pikkarainen S, Piuhola J, Rysa J, Toth M, Ruskoaho H (2002) Apelin, the novel endogenous ligand of the orphan receptor APJ, regulates cardiac contractility. *Circ Res* **91:** 434–440

Takakura N, Huang XL, Naruse T, Hamaguchi I, Dumont DJ, Yancopoulos GD, Suda T (1998) Critical role of the TIE2 endothelial cell receptor in the development of definitive hematopoiesis. *Immunity* **9:** 677–686

Takakura N, Watanabe T, Suenobu S, Yamada Y, Noda T, Ito Y, Satake M, Suda T (2000) A role for hematopoietic stem cells in promoting angiogenesis. *Cell* **102:** 199–209

Tatemoto K, Hosoya M, Habata Y, Fujii R, Kakegawa T, Zou MX, Kawamata Y, Fukusumi S, Hinuma S, Kitada C, Kurokawa T, Onda H, Fujino M (1998) Isolation and characterization of a novel endogenous peptide ligand for the human APJ receptor. *Biochem Biophys Res Commun* **251:** 471–476

Tatemoto K, Takayama K, Zou MX, Kumaki I, Zhang W, Kumano K, Fujimiya M (2001) The novel peptide apelin lowers blood pressure via a nitric oxide-dependent mechanism. *Regul Pept* **99:** 87–92

Thurston G, Wang Q, Baffert F, Rudge J, Papadopoulos N, Jean-Guillaume D, Wiegand S, Yancopoulos GD, McDonald DM (2005) Angiopoietin 1 causes vessel enlargement, without angiogenic

sprouting, during a critical developmental period. *Development* **132:** 3317–3326

Wang HU, Chen ZF, Anderson DJ (1998) Molecular distinction and angiogenic interaction between embryonic arteries and veins revealed by ephrin-B2 and its receptor Eph-B4. *Cell* **93:** 741–753

Yamada Y, Takakura N (2006) Physiological pathway of differentiation of hematopoietic stem cell population into mural cells. *J Exp Med* **203:** 1055–1065

Zhong TP, Childs S, Leu JP, Fishman MC (2001) Gridlock signalling pathway fashions the first embryonic artery. *Nature* **414:** 216–220

EphB4 Overexpression in B16 Melanoma Cells Affects Arterial-Venous Patterning in Tumor Angiogenesis

Xiaoyong Huang,[1,2] Yoshihiro Yamada,[2] Hiroyasu Kidoya,[2] Hisamichi Naito,[2] Yumi Nagahama,[2] Lingyu Kong,[2] Shin-Ya Katoh,[2] Weng-lin Li,[1] Masaya Ueno,[2] and Nobuyuki Takakura[2]

[1]Department of Stem Cell Biology, Cancer Research Institute, Kanazawa University, Kanazawa, Japan and [2]Department of Signal Transduction, Research Institute for Microbial Diseases, Osaka University, Suita-shi, Osaka, Japan

Abstract

EphB4 receptor and its ligand ephrinB2 play an important role in vascular development during embryogenesis. In blood vessels, ephrinB2 is expressed in arterial endothelial cells (EC) and mesenchymal supporting cells, whereas EphB4 is only expressed in venous ECs. Previously, we reported that OP9 stromal cells, which support the development of both arterial and venous ECs, in which EphB4 was overexpressed, could inhibit ephrinB2-positive (ephrinB2$^+$) EC development in an embryonic tissue organ culture system. Although the EphB4 receptor is expressed in a variety of tumor cells, its exact function in regulating tumor progression has not been clearly shown. Here we found that overexpression of EphB4 in B16 melanoma cells suppressed tumor growth in a s.c. transplantation tumor model. Histologic examination of these tumors revealed that EphB4 overexpression in B16 cells selectively suppressed arterial ephrinB2$^+$ EC development. By coculturing ephrinB2-expressing SV40-transformed mouse ECs (SVEC) with EphB4-overexpressing B16 cells, we found that EphB4 induced the apoptosis of SVECs. However, ephrinB2 did not induce the apoptosis of EphB4-overexpressing B16 cells. Based on results from these experiments, we concluded that EphB4 overexpression in B16 tumor cells suppresses the survival of arterial ECs in tumors by a reverse signaling via ephrinB2. [Cancer Res 2007;67(20):9800–8]

Introduction

The growth of solid tumors is closely associated with the ability to recruit blood vessels, which can supply tumors with the growth factors, oxygen, and nutrients necessary for their survival and growth and for the maintenance of the malignant state. In embryos, blood vessels are initially formed by a process called vasculogenesis but become remodeled and mature through a second process called angiogenesis, which results in the development of a highly hierarchical architecture of blood vessels ranging from small to large (1). During these processes, a distinction develops between arterial and venous endothelial cells (EC); eventually, the arterial ECs selectively express ephrinB2 and the venous ECs preferentially express EphB4, which is a cognate receptor tyrosine kinase for ephrinB2 (2–4).

Eph receptors and ephrins are frequently expressed in reciprocal patterns that correlate with cellular boundaries during embryonic development (5). Consistent with this expression pattern, Eph-ephrin signaling regulates the boundary of distinct cells in culture (6) and is required for vascular modeling (2, 7), axon guidance (8, 9), and epithelial-mesenchymal transitions (10). Reciprocal expression of ephrinB2 and EphB4 in arterial and venous ECs, respectively, suggests that ephrinB2 and EphB4 might interact at the arterial-venous interface and regulate angiogenesis (2–4). Targeted disruption of either ephrinB2 or EphB4 in mice has been shown to lead to early embryonic lethality through the disruption of blood vessel formation in angiogenesis but not in vasculogenesis (2–4). EphrinB2 contains transmembrane and cytoplasmic domains; therefore, it has been suggested that the functioning of this receptor/ligand system is dependent on cell-to-cell contact (5). EphB4 is a member of the receptor tyrosine kinase family and initiates signal transduction through autophosphorylation after ligand binding (forward signaling); however, in contrast to other soluble ligands for receptor system, ephrinB2 also has the ability to initiate receptor-like active signaling (reverse signaling; refs. 5, 11, 12). Indeed, a loss-of-function experiment, in which the cytoplasmic domain of ephrinB2 was deleted, showed that bidirectional EphB4/ephrinB2 signaling was required for proper arterial and venous development (13).

It was originally assumed that the blood vessel system in tumors was composed of homogeneous capillaries, based on their uniformly small size and the sparse adhesion of mural cells to ECs. However, it has been reported that the vessels in tumors can be divided into ephrinB2-positive (ephrinB2$^+$) arterial and ephrinB2-negative (ephrinB2$^-$), and therefore presumably, venous ones (7). This suggests that the EphB4/ephrinB2 system is involved in tumor angiogenesis and that it may have an affect on the specification of arteries and veins in the tumor environment. Moreover, EphB4 expression has been reported in numerous tumors such as breast, liver, gastrointestinal, prostate, bladder, lung, and ovarian cancers, as well as leukemia, mesothelioma, and melanoma (14–19). Recent research reported that reduction of EphB4 activity accelerated tumorigenesis in the colon and rectum and that loss of EphB4 expression represented a critical step in colorectal cancer progression (15). Furthermore, a highly significant correlation was reported between EphB4 positivity and low histologic grading of tumor cells in breast cancer (20). Other reports also showed that overexpression of EphB4 is inversely related to a poor prognosis in head and neck squamous cell carcinoma and endometrial carcinoma (21, 22). These results indicated that EphB4 expression is not compatible with tumor progression. However, in mesothelioma, up-regulation of EphB4 was shown to provide a survival advantage in tumor tissue (17)

Note: Supplementary data for this article are available at Cancer Research Online (http://cancerres.aacrjournals.org/).

Requests for reprints: Nobuyuki Takakura, Department of Signal Transduction, Research Institute for Microbial Diseases, Osaka University, 3-1 Yamada-oka, Suita, Osaka 565-0871, Japan. Phone: 81-6-6879-8316; Fax: 81-6-6879-8314; E-mail: ntakaku@biken.osaka-u.ac.jp.

doi:10.1158/0008-5472.CAN-07-0531

and resulted in growth of the tumor. At present, little is known about this apparent discrepancy in terms of the function of EphB4 in tumor progression, but it is possible that coexpression of another member of the EphB family, such as EphB1, EphB2, EphB3, and EphB6, or coexpression of EphB4 ligands such as ephrinB2 in tumor cells may affect tumor cell viability and proliferation. Indeed, it was reported that, in mesothelioma, ephrinB2 and EphB4 were almost exclusively coexpressed in cells from tumor cell lines and primary cancers, and that knockdown of either ephrinB2 or EphB4 by small interfering RNA inhibited the viability of tumor cells coexpressing EphB4/ephrinB2 (17). This suggested that the expression of ephrinB2 in tumor cells has a reciprocal affect on EphB4 expression in an autocrine or paracrine manner. Similar coexpression of this receptor-ligand pair has been reported in other tumor types, including endometrial, lung, and colon carcinoma, both in the corresponding tumor cell lines and primary cancers (16, 23, 24).

Although the expression of EphB4 in various tumors and its effect on tumor progression have been reported, its other role in the development of arteries and veins in tumors has not been clarified. To investigate this, we searched for tumor cells that expressed EphB4 on their surface, but not ephrinB2, to exclude any autocrine or paracrine effects of EphB4 on tumor cells. Furthermore, we looked for murine tumor cell lines because of the availability of an *in vivo* tumor angiogenesis model, in which murine EphB4 affects murine ephrinB2 of ECs. Among tumor cell lines tested, such as melanoma, colon cancer, lung cancer, and mammary gland tumor, we found a B16 mouse melanoma cell line that matched these criteria. Using this cell line, we overexpressed or knocked down EphB4 and observed the effect of EphB4 on blood vessel formation and tumor growth. Moreover, to test the viability of ephrinB2$^+$ ECs on stimulation with EphB4$^+$ tumor cells, we cocultured an ephrinB2-induced EC line, a SV40-transformed mouse EC line (SVEC; ref. 25), with B16 melanoma cells *in vitro*, and observed dose dependency of cell-surface EphB4 and apoptosis of ephrinB2$^+$ ECs.

Materials and Methods

Animals. C57BL/6 mice and Wistar rats were purchased from Japan SLC at 8 weeks of age and used between 8 and 12 weeks of age. EphB4$^{LacZ/+}$ and ephrinB2$^{LacZ/+}$ mice (2, 4) were provided by Dr. D.J. Anderson (California Institute of Technology, Pasadena, CA). Animal care in our laboratory was in accordance with the guidelines of Kanazawa and Osaka University for animal and recombinant DNA experiments.

Cell lines and transfection. B16 (mouse melanoma) cells were cultured in DMEM supplemented with 10% FCS. BaF3 pre-B hematopoietic cells were cultured in RPMI 1640 supplemented with 10% FCS and 1 ng/mL interleukin-3.

Transfection of mouse full-length *EphB4* or *ephrinB2* cDNA (26) was done using Lipofectamine Plus reagent (Invitrogen). Stable transfection was obtained by antibiotic resistance selection using G418 (Life Technologies, Inc.). Stable knockdown of *EphB4* gene in B16 cells was done using the short hairpin RNA (shRNA) method. shRNA coding for *EphB4* was introduced into the pSINsi-hU6 DNA vector (Takara) at the *Bam*H1 and *Cla*1 ligation sites according to the manufacturer's instruction. shRNA oligonucleotides were synthesized corresponding to the published sequence of *EphB4* mRNA (NM_010144). The insert for *EphB4* shRNA (forward strand, 5′-GCATCACAGTCAGACTCAACT-3′; reverse strand, 5′-AGTTGAGTCTGACTGTGATGC-3′) and a nonspecific oligonucleotide insert for negative control (forward strand, 5′-gatccGATCGTTGGTGTGGTGGGTCGttcaagagaACTACCATGCTCCCATGAACAttttttat-3′; reverse strand, 5′-cgataaaaaaTGTTCATGGGAGCATGGTAGTtctcttgaaCGACCCACCACACCAACGATCg-3′) were used. Plasmids were transfected into B16 by electroporation (Amaxa Biosystems); 48 h after electroporation, the cells were harvested by trypsin-EDTA (Life Technologies) and reseeded at a density of 2×10^4 cells in 10-cm culture dishes. The following day, geneticine (Life Technologies) was added to a final concentration of 1,000 μg/mL. Eight days after addition of geneticine, colonies were picked with a cloning ring (Asahi Techno Glass) and reseeded in the culture plate. For the evaluation of *EphB4* knockdown, *EphB4* expression was determined by real-time reverse transcription and reverse transcription-PCR (RT-PCR).

RT-PCR analysis. Total RNA was extracted from cells using the RNeasy plus mini kit (Qiagen) according to the manufacturer's protocol. Total RNA was reverse transcribed into cDNA using Exscript RT Reagent Kit (Takara). Primer pairs for studying the expression of mouse *EphB4*, mouse *ephrinB2*, human *EphB4*, human *ephrinB2*, mouse *β-actin*, or human *glyseraldehyde-3-phosphate dehydrogenase* (*GAPDH*) were, for real-time PCR, *EphB4* (sense, 5′-AATGTCACCACTGACCGTGA-3′; antisense, 5′-TCAGGAAACGAACACTGCTG-3′) and *GAPDH* (sense, 5′-TGGCAAAGTGGAGATTGTTGCC-3′; antisense, 5′-AAGATGGTGATGGGCTTCCCG-3′), and for RT-PCR primers, mouse *EphB4* (sense, 5′-CGTCCTGATGTCACCTATACCTTTGAGG-3′; antisense, 5′-GAGTACTCAACTTCCCTCCCATTGCTCT-3′), mouse *ephrinB2* (sense, 5′-AGGAATCACGGTCCAACAAG-3′; antisense, 5′-GTCTCCTGCGGTACTTGAGC-3′), human *EphB4* (sense, 5′-GGCTGCTCGCAACATCCTAGT-3′; antisense, 5′-CCACATCACAATCCCGTAAC-3′), human *ephrinB2* (sense, 5′-CTGCTGGATCAACCAGGAAT-3′; antisense, 5′-GATGTTGTTCCCCGAATGTC-3′), mouse *β-actin* (sense, 5′-CCTAAGGCCAACCGTGAAAAG-3′; antisense, 5′-TCTTCATGGTGCTAGGAGCCA-3′), and human *GAPDH* (sense, 5′-GAAGGTGAAGGTCGGAGTC-3′; antisense, 5′-GAAGATGGTGATGGGATTTC-3′). Real-time PCR analysis was done with Platinum SYBR Green qPCR SuperMix-UDG (Invitrogen). The levels of PCR products were monitored with an ABI PRISM 7900HT sequence detection system and analyzed with ABI PRISM 7900 SDS software (Applied Biosystems). The adjustment of baseline and threshold was done according to the manufacturer's instructions. The relative abundance of transcripts was normalized to the constitutive expression level of *GAPDH* RNA.

Generation of EphB4 monoclonal antibody. The extracellular ligand binding domain of mouse *EphB4* (amino acids 39–165) was cloned into pGEX-2T to generate glutathione *S*-transferase (GST)–fused protein. EphB4 ligand binding domain expressed as a GST fusion protein in DH5α *E. coli* was purified by affinity chromatography and used as an immunogen for Wistar rats. The methods for generation of hybridoma cells using X63Ag8 mouse myeloma cells and the purification of monoclonal antibody (mAb) were the same as previously described (27). The sensitivity of the mAb produced from the hybridoma clone (VEB4-7E4) was confirmed by Western blotting and fluorescence-activated cell sorting (FACS) analysis with BaF3 cells stably transfected with EphB4 (BaF3/EphB4). Furthermore, by immunohistochemistry, the specificity of the mAb was examined by reciprocal expression of ephrinB2 and EphB4 or colocalization of ECs stained with anti–β-galactosidase and anti-EphB4 antibody on the hind limb section of ephrinB2$^{Lac/+}$ or EphB4$^{Lac/+}$ mice, respectively.

Immunoprecipitation and Western blotting. Cells were lysed on ice with lysis buffer [50 mmol/L HEPES (pH 7.4), 1% Triton X-100, 10% glycerol, 10 mmol/L sodium pyrophosphate, 100 mmol/L sodium fluoride, 4 mmol/L EDTA, 2 mmol/L sodium orthovanadate, 50 μg/mL aprotinin, 1 mmol/L phenylmethylsulfonyl fluoride, 100 mmol/L leupeptin, 25 μmol/L pepstatin A]. Cell lysates were cleared by centrifugation for 15 min at 15,000 × *g* at 4°C, and then proteins were subjected to SDS-PAGE and transferred onto polyvinylidene difluoride membranes (Nihon Millipore). Membranes were blocked with 5% normal goat serum, 1% bovine serum albumin, 5% skimmed milk in TBST [20 mmol/L Tris (pH 7.4), 150 mmol/L sodium chloride, 0.1% Tween 20] for 60 min at room temperature. Membranes were washed and then incubated for 60 min at room temperature with anti-EphB4 mAb or anti-ephrinB2 polyclonal antibody (Santa Cruz Biotechnology), followed by 60 min at room temperature with horseradish peroxidase–conjugated goat anti-mouse immunoglobulins (Amersham Pharmacia Biotech) or goat anti-rabbit immunoglobulins antibody (Biosourse). Proteins were visualized by enhanced chemiluminescence detection system (LAS-3000 mini, Fuji).

FACS analysis. Flow cytometric analysis was done as previously described (28). The antibodies used in this experiment were anti-EphB4 mAb (VEB4-7E4) and Alexa Fluor 488 goat anti-rat immunoglobulin G (IgG) (H+L) antibody (Molecular Probes). For the analysis of specific binding of EphB4 mAb to EphB4 on BaF3/EphB4 cells, cells were preincubated with soluble EphB4 receptor (sEphB4; extracellular domain of EphB4 fused with human Fc of IgG; ref. 26) for 30 min on ice. The stained cells were analyzed by FACSCalibur (Becton Dickinson).

Immunohistochemistry. Tissue fixation, preparation of tissue sections, and staining of sections with antibodies were done as previously described (29). Antibodies used in immunohistochemical staining were nonlabeled or FITC-conjugated anti-platelet/endothelial cell adhesion molecule 1 (PECAM-1) mAb (PharMingen), anti-β-galactosidase antibody (Chemicon), and anti-EphB4 mAb (VEB4-7E4). Secondary antibodies used were horseradish peroxidase- or Alexa Fluor 488-conjugated goat anti-rat IgG(H+L) antibody for anti-EphB4 mAb (Biosource) and nonlabeled anti-PECAM-1 mAb or HRP-, alkaline phosphatase-, or Alexa Fluor 546-conjugated goat anti-rabbit IgG antibody (Molecular Probes) for anti-β-galactosidase antibody. Anti-PECAM-1 antibody was developed with HRP-conjugated anti-rat IgG antibody (Biosource). For color reaction of HRP, samples were soaked in PBS containing 250 μg/mL diaminobenzidine (Dojin Chem.) in the presence of 0.05% $NiCl_2$ for 10 min, and 0.01% hydrogen peroxidase was added for the enzymatic reaction. For the color reaction of alkaline phosphatase, new Fuchsin substrate kit (DAKO) was used. Nuclear staining was done with Hoechst (Sigma) or 4′,6-diamidino-2-phenylindole (DAPI; Invitrogen) to obtain fluorescent images. Finally, the sections were observed and photographed under a microscope (IX-70, Olympus) with UV lamp.

***In vitro* proliferation assay.** Cells (10^3 per well) were seeded into 96-well plates and cultured in DMEM supplemented with 10% FCS under 37°C, CO_2 0.5%. The cell number was counted daily.

Mouse xenograft assay. Tumor cells (5×10^6 per mouse in 0.1-mL PBS) were injected s.c. into 8-week-old female wild-type C57BL/6, ephrinB2$^{LacZ/+}$, or EphB4$^{LacZ/+}$ mice, as previously reported (30). Tumor volumes were measured with calipers every 3 days and calculated as width × width × length × 0.52. Tumor tissues were removed from mice on day 18 postinjection.

Coculture system and apoptosis assay. B16/mock (B16 cells induced with mock vector) or B16/EphB4 (B16 cells induced with mouse EphB4 expression vector) tumor cells labeled with PKH26 Red Fluorescent Cell Linker Mini Kit (Sigma) were seeded into 12-well plates in culture medium (DMEM supplemented with 10% FCS). When cells had reached 80% confluency, they were serum starved for 12 h in DMEM. SVECs transduced with mouse ephrinB2 (SVEC/ephrinB2 cells) were prelabeled with PKH67 Green Fluorescent Cell Linker (Sigma) and serum starved for 12 h in DMEM, and then added in medium (DMEM, 2% FCS) either into B16/mock or B16/EphB4 tumor cells or trans-well plates with 0.4-μm pores (Corning, Inc.). For binding inhibition assays of EphB4 in B16/EphB4 cells and ephrinB2 in SVEC/ephrinB2 cells, soluble EphB4-Fc (sEphB4; 5 μg/mL) was added. After 24 h of coculture, cells were harvested from the culture plate using trypsin-EDTA and stained with Annexin V-Cy5 Apoptosis Detection Kit (BioVision) and DAPI (Invitrogen). Stained cells were analyzed by flow cytometry with UV laser (JSAN, Bay bioscience).

Statistical analysis. All date are presented as mean ± SE. For statistical analysis, Microsoft Excel software was used for two-sided Student's *t* test.

Results

Generation of mAb against mouse EphB4. To investigate EphB4 expression at the protein level in tumor cells, we generated antimouse EphB4 mAb (clone VEB4-7E4) and first observed EphB4 expression in the BaF3 hematopoietic cell line induced with ectopic EphB4 (BaF3/EphB4, Fig. 1*A*) by flow cytometric analysis (Fig. 1*B*) and Western blotting (Fig. 1*C*). As observed in Fig. 1*B*, this mAb recognized EphB4 on BaF3 cells and this reaction to EphB4 by the mAb was almost completely suppressed by soluble EphB4 protein, suggesting that this reaction was specific to EphB4. Moreover, this mAb could recognize a 120-kDa protein from BaF3/EphB4 cell lysates but not from BaF3/mock cells (Fig. 1*C*). In immunohistochemical staining of hind limb muscle using LacZ reporter strain to detect expression of ephrinB2 (arteries; ref. 4), together with antibody to CD31/PECAM-1, a pan-endothelial marker, this mAb against EphB4 (VEB4-7E4) did not recognize CD31$^+$ephrinB2$^+$ arterial ECs but was able to mark CD31$^+$ephrinB2$^-$ ECs (Fig. 1*D*). These reciprocal expression profiles indicated that this mAb could

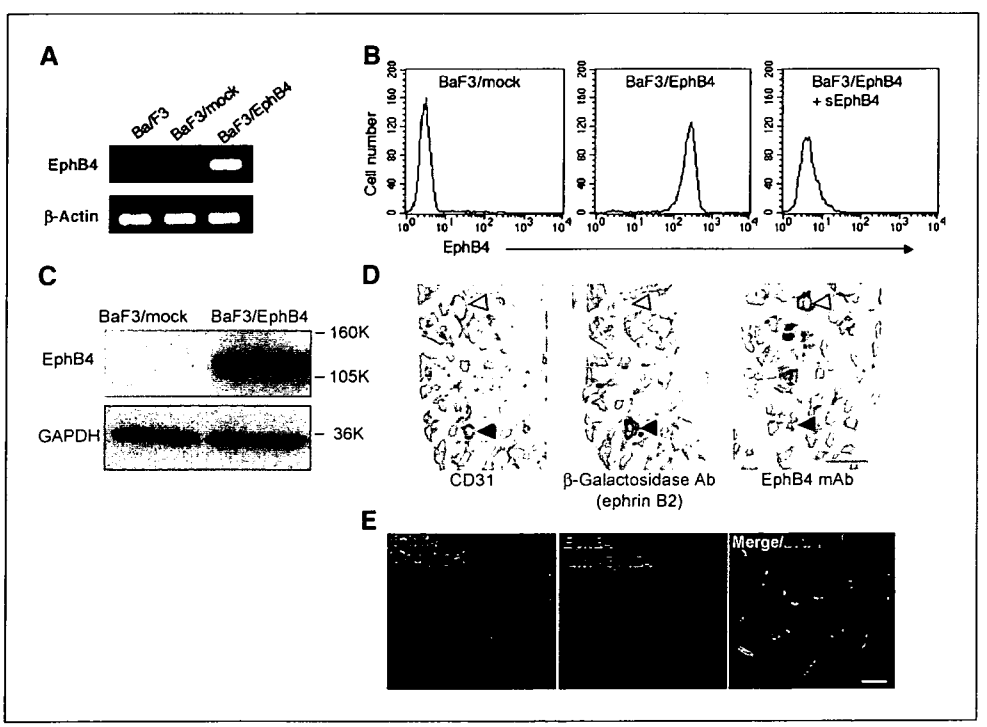

Figure 1. Specificity of generated EphB4 mAb. *A*, RT-PCR analysis of *EphB4* mRNA in BaF3 cells, BaF3 cells transfected with mock (BaF3/mock), or *EphB4* (BaF3/EphB4) plasmid. *B*, FACS analysis of EphB4 expression in BaF3/mock and BaF3/EphB4 cells. Soluble EphB4-FC chimeric protein (sEphB4) was used for analyzing specific binding of EphB4 mAb to EphB4. *C*, Western blotting analysis for detecting EphB4 protein from cell lysates of BaF3/mock or BaF3/EphB4 with EphB4 mAb and anti-GAPDH antibody. *D*, serial sections from mouse hind limb muscle of 8-week-old ephrinB2$^{LacZ/+}$ mice were stained with anti-CD31, anti-β-galactosidase, or anti-EphB4 antibodies. *Open* and *closed arrows*, CD31$^+$ephrinB2$^-$EphB4$^+$ and CD31$^+$ephrinB2$^+$EphB4$^-$ blood vessels, respectively. *Bar*, 40 μm. *E*, sections from mouse hind limb muscle of 8-week-old EphB4$^{LacZ/+}$ mice were stained with anti-β-galactosidase and anti-EphB4 antibodies. Nuclei were stained with DAPI. *Bar*, 40 μm.

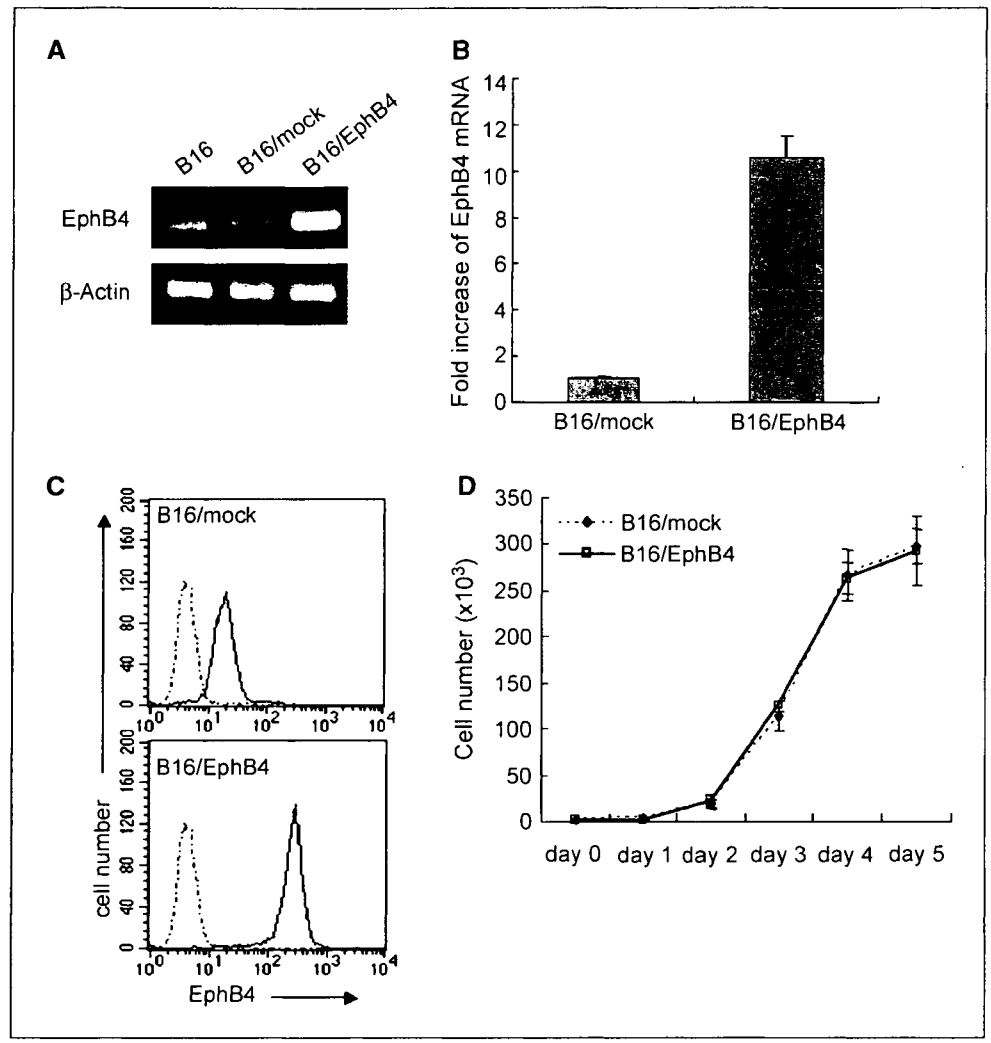

Figure 2. Effect of EphB4 overexpression in B16 cells on *in vitro* proliferation. B16 cells were transfected with mock (B16/mock) or *EphB4* (B16/EphB4) expression vectors. *A*, RT-PCR analysis of *EphB4* mRNA expression in B16, B16/mock, or B16/EphB4 cells. *B*, real-time PCR analysis of *EphB4* mRNA in B16/mock or B16/EphB4 cells. *C*, FACS analysis of *EphB4* protein expression by EphB4 mAb in B16/mock or B16/EphB4 cells. *Dashed line*, intensity of negative control. *D*, *in vitro* proliferation analysis.

react with EphB4. Moreover, to detect the expression of EphB4 in hind limb muscle from LacZ reporter mice (2), β-galactosidase–positive ECs were exclusively stained with anti-EphB4 antibody (Fig. 1*E*). Taken together, we concluded that this mAb (VEB4-7E4) reacts specifically with EphB4.

EphB4 overexpression did not alter *in vitro* proliferation of B16 melanoma cells. We looked for a tumor cell line that endogenously expresses EphB4 but not ephrinB2. Among several mouse and human tumor cell lines tested, we found that B16 mouse melanoma cells matched these criteria (Supplementary Table S1). Therefore, using B16 melanoma cells, we first observed whether overexpression of EphB4 in B16 cells affects cell growth. Overexpression of EphB4 stably transduced in B16 cells (B16/EphB4) was compared with that in control B16 cells transduced with mock vector (B16/mock) by RT-PCR (Fig. 2*A*) and real-time PCR (Fig. 2*B*) analyses at the mRNA level. Overexpression of EphB4 in B16/EphB4 cells was also confirmed by FACS analysis at the protein level (Fig. 2*C*). An *in vitro* proliferation of B16/EphB4 and B16/mock cells was observed. Results indicated that B16 overexpression did not alter the growth of B16 cells (Fig. 2*D*). We cloned several EphB4-overexpressing B16 cells and there was no difference from the results obtained with the subclones (data not shown).

EphB4 overexpression suppressed tumor growth in *in vivo* xenograft assay. To investigate the function of EphB4 in B16 cells *in vivo*, B16/EphB4 and B16/mock cells were injected s.c. into C57BL/6 mice. To observe tumor growth, the tumor size was measured every 3 days. Eighteen days after inoculation of tumor cells, the tumors were removed from the mice and the tumor mass was weighed. Although EphB4 overexpression did not affect the *in vitro* growth of B16 cells (see above), the *in vivo* growth of B16/EphB4 cells was clearly inhibited in comparison with that of B16/mock cells (Fig. 3*A*).

Although EphB4 protein expression level in parental B16 cells was low (Fig. 2*C*), to confirm dose dependency of EphB4 in tumor growth, we knocked down the *EphB4* gene in B16 cells and then studied *in vitro* and *in vivo* growth. As shown in Fig. 3*B*, on transfection with plasmids containing shRNA oligonucleotides that specifically recognized *EphB4* sequences, *EphB4* expression of B16 cells (B16/shRNA) was reduced compared with the level of expression when the cells were transfected with a plasmid containing nonspecific shRNA (B16/scr). *In vitro* cell proliferation was not affected by the depletion of EphB4 from B16 cells (Fig. 3*B*, *middle*); however, we confirmed that, *in vivo*, EphB4 depletion in B16 cells enhanced tumor growth (Fig. 3*B*, *right*). These results clearly indicated that reduction of EphB4 expression accelerates tumor growth in B16 cells.

EphB4 overexpression in B16 cells inhibits formation of blood vessels with an arterial phenotype in tumors. To clarify the

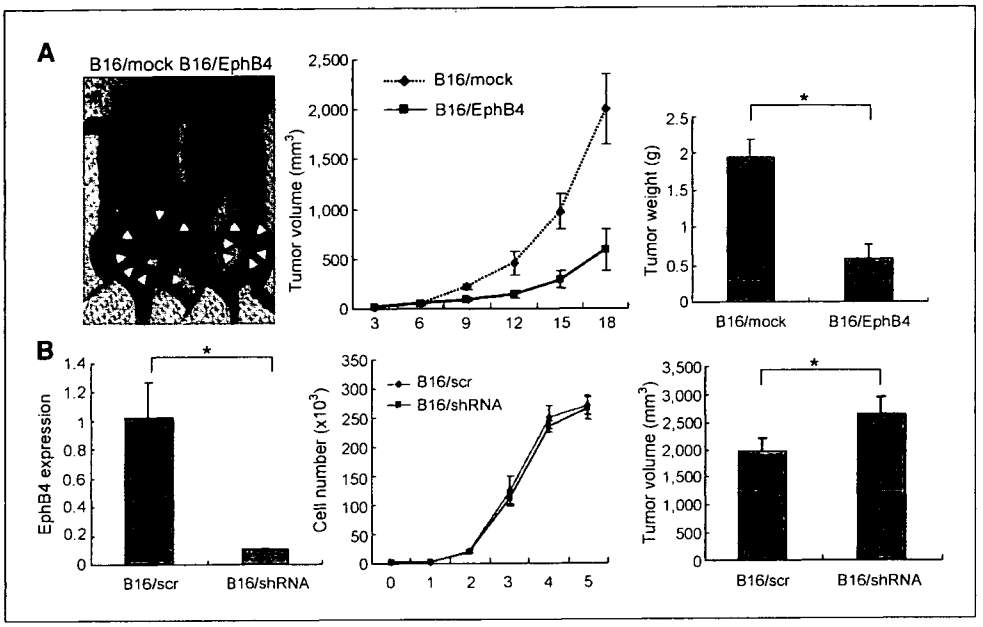

Figure 3. Tumor growth in inverse proportion to the expression levels of EphB4. *A, left,* gross appearance of tumors derived from B16/mock or B16/EphB4 cells on day 18 after tumor cell inoculation. *Arrows,* tumor area. *Middle,* tumor volume measured every 3 d after tumor cell inoculation. *Right,* tumor weight on day 18 after tumor cell inoculation. *, $P < 0.05$ ($n = 5$). *B, left,* real-time RT-PCR analysis of *EphB4* mRNA expression in B16 cells transduced by an *EphB4*-specific shRNA (B16/shRNA) or a nonspecific insert (B16/scr). *, $P < 0.05$ ($n = 3$). *Middle, in vitro* proliferation analysis. *Right,* tumor volume was determined on day 18 after s.c. inoculation of B16/shRNA or B16/scr cells into C57BL/6 mice. *, $P < 0.05$ ($n = 5$).

suppressive effect on tumor growth of EphB4 overexpression in B16 cells, we stained tumor tissues with anti-CD31 antibody and found that the number of blood vessels in tumors from B16/EphB4 cells was almost half that found in tumors from B16/mock cells (Fig. 4*A* and *B*). On the other hand, the difference in vessel density between B16/mock and B16/shEphB4 was not large compared with that between B16/mock and B16/EphB4; however, vessel density was slightly, but statistically significantly, higher in the B16/shEphB4 tumor than in the control B16/mock tumor (Fig. 4*A* and *B*).

These results suggested that EphB4 overexpression in B16 cells suppressed tumor angiogenesis.

Nevertheless, the method by which EphB4 affects blood vessel development was not clear. To investigate the properties of blood vessels in tumors, we inoculated B16/EphB4 and B16/mock cells s.c. into LacZ reporter mice to detect the expression of ephrinB2 (4) or EphB4 (2), together with anti-CD31 antibody, in tumor sections. As shown in Fig. 5, in tumors derived from B16/mock cells, nearly half of the ECs were ephrinB2$^+$ and had an arterial phenotype. On

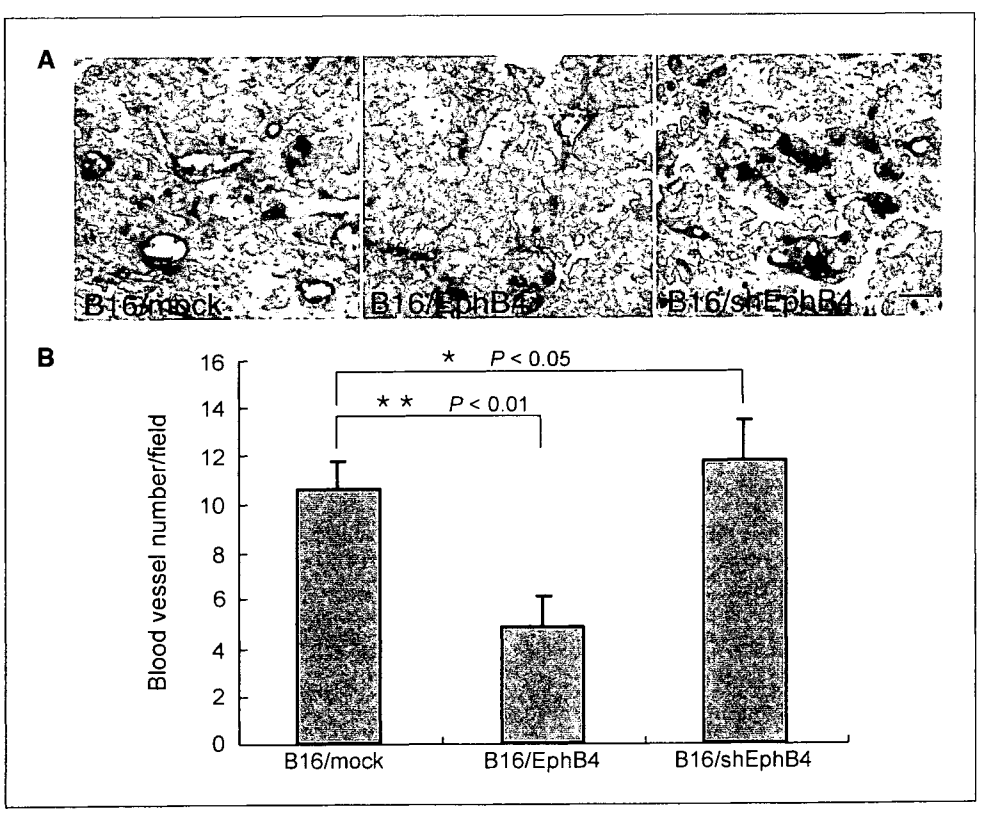

Figure 4. Effect of EphB4 overexpression in B16 cells on tumor angiogenesis. *A,* blood vessel formation in tumors derived from B16/mock (*left*), B16/EphB4 (*middle*), or B16/shEphB4 (*right*) cells. Sections were obtained from the tumors on day 18 after inoculation with the respective tumor cells and stained with anti-CD31 mAb (*red*). *Bar,* 40 μm. *B,* quantitative evaluation of blood vessels from 30 random fields of three independent tumors, as indicated. *, $P < 0.05$; **, $P < 0.01$.

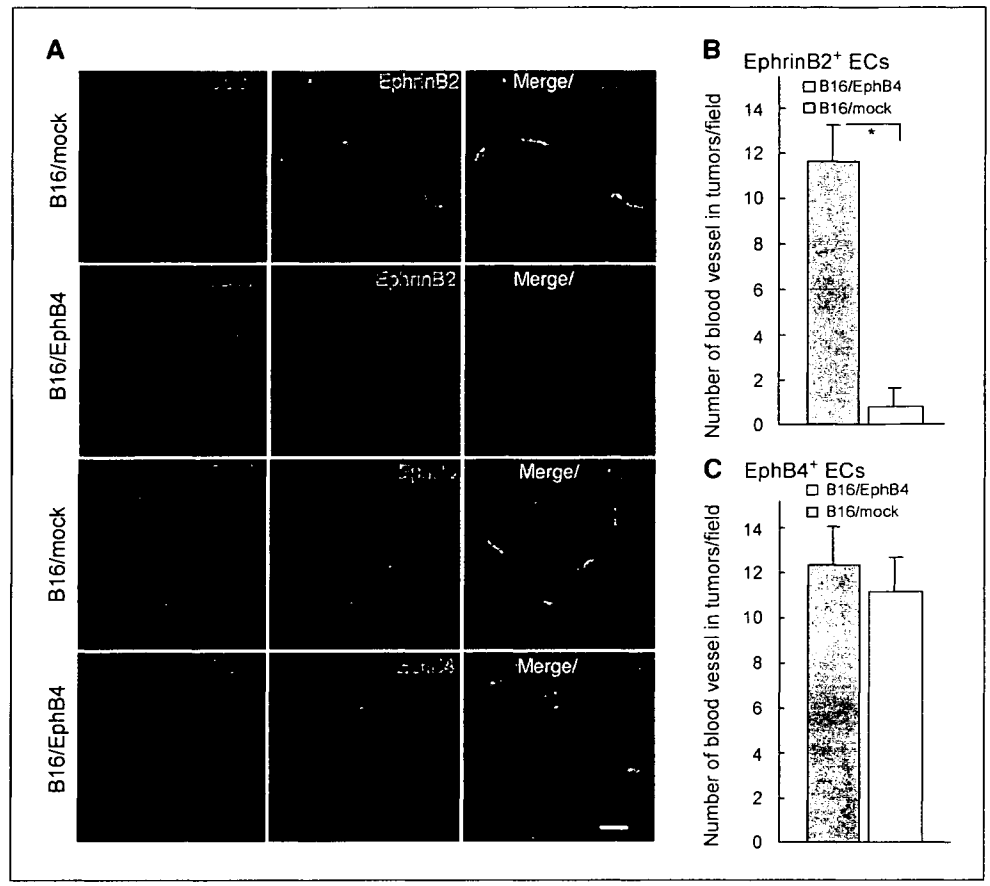

Figure 5. Effect of EphB4 overexpression in B16 cells on the arterial-venous patterning in tumors. *A*, sections derived from tumors generated by s.c. inoculation of B16/mock (*top lane*) or B16/EphB4 (*second lane*) into ephrinB2$^{LacZ/+}$ mice for 18 d were doubly stained with anti-CD31 (*red*) and anti–β-galactosidase (*green*) antibodies. Merged image with CD31 and β-galactosidase staining was shown as indicated. Nuclei were counterstained with Hoechst. Sections derived from tumors generated by s.c. inoculation of B16/mock (*third lane*) or B16/EphB4 (*bottom lane*) into EphB4$^{LacZ/+}$ mice after 18 d were doubly stained with anti-CD31 (*red*) and anti–β-galactosidase (*green*) antibodies. Merged image with CD31 and β-galactosidase staining was shown as indicated. Nuclei were counterstained with Hoechst. *Bar*, 40 μm. *B* and *C*, quantitative evaluation of ephrinB2$^+$ arteries (*B*) or EphB4$^+$ veins (*C*) from 30 random fields of three independent tumors, as indicated. *, $P < 0.05$.

the other hand, in B16/EphB4 tumors, ephrinB2$^+$ ECs were difficult to detect; only ~6% of ECs in these tumors expressed ephrinB2. By contrast, EphB4$^+$ ECs having a venous phenotype were observed in equal numbers in tumors derived from both B16/mock and B16/EphB4 cells. Therefore, we concluded that EphB4 in B16 cells selectively suppressed the formation of blood vessels with an arterial phenotype.

EphB4 in B16 cells induces apoptosis of ephrinB2$^+$ ECs. Because EphB4 suppressed the appearance of ephrinB2$^+$ ECs in tumors, the final aspect we investigated was how EphB4 overexpression in B16 cells might be affecting ephrinB2$^+$ cells *in vitro*. To achieve this, we induced ephrinB2 into the murine SVEC EC line and generated stably and strongly ephrinB2-expressing ECs (SVEC/ephrinB2), because endogenous ephrinB2 expression was weak in the original SVECs (Supplementary Fig. S1), and cocultured these cells with B16/mock or B16/EphB4 cells (Fig. 6). After coculturing for 24 h, apoptosis of SVEC/ephrinB2 in B16/mock cells or B16/EphB4 cells, B16/mock cells cocultured with SVEC/ephrinB2, and B16/EphB4 cells cocultured with SVEC/ephrinB2 cells was observed by staining with Annexin V and nuclear dye DAPI (Fig. 6*A* and *B*). Results showed that B16/EphB4 cells enhanced apoptosis (Annexin V$^+$DAPI$^-$) and cell death (Annexin V$^+$DAPI$^+$) in SVEC/ephrinB2 cells compared with B16/mock cells (Fig. 6*A* and *B*). When compared with cell death of SVEC/ephrinB2 in B16/mock cells, similar apoptosis and cell death of SVEC/ephrinB2 cells in normal culture conditions (i.e., SVEC/ephrinB2 cells not cocultured with B16 cells) was observed (data not shown). The apoptotic effect of B16/EphB4 cells on SVEC/ephrinB2 cells in this coculturing system was suppressed by the separation of the two cell types by means of a 0.4-μm-pore filter (Fig. 6*A* and *B*). Moreover, blockade of interactions between SVEC/ephrinB2 and B16/EphB4 cells with soluble EphB4 proteins abolished the B16/EphB4-mediated increase in cell death of SVEC/ephrinB2 (Fig. 6*A* and *B*). Therefore, we concluded that apoptosis of SVEC/ephrinB2 cells was accelerated by cell-to-cell contact with B16/EphB4 cells.

On the other hand, in the case of B16 cells, the percentage (Fig. 6*A* and *B*) and absolute cell number (data not shown) of apoptotic and dead cells from B16/EphB4 cells cocultured with SVEC/ephrinB2 cells were not statistically significantly different compared with those from B16/mock cells cocultured with SVEC/ephrinB2 cells. Moreover, such apoptosis and cell death was also observed in B16/mock and B16/EphB4 under normal culture conditions without coculturing with SVEC/ephrinB2 cells (data not shown). This suggested that ephrinB2 does not affect EphB4 in B16 cells, in terms of cell viability, as a forward signaling.

Taken together, we concluded that EphB4 overexpression in B16 melanoma cells induces cell apoptosis of ephrinB2$^+$ ECs. Therefore, when inoculated into mice, B16/EphB4 cells might suppress the survival of ephrinB2$^+$ ECs, resulting in insufficient arterial-venous blood vessel distribution and the inhibition of tumor growth.

Discussion

Although the EphB4 receptor has been reported to be expressed in various tumor cells (14–19), its exact function in arterio-venous specification has not yet been elucidated. In this study, we showed

that EphB4 overexpression in B16 melanoma cells suppressed tumor angiogenesis, especially the development of ephrinB2$^+$ ECs with an arterial phenotype in tumors. By coculturing ephrinB2-expressing ECs (SVEC induced with ephrinB2) with EphB4-overexpressing B16 cells, we found that EphB4 reverse signaling via ephrinB2 was involved in the apoptosis of ephrinB2$^+$ ECs. Ideally, it was better to coculture ephrinB2$^+$ ECs in tumors derived from B16 cells with B16/EphB4 cells to examine the nature of the arterial ECs affected by EphB4 in tumor cells. However, due to technical problems, we experienced difficulties in culturing primary ECs from tumors *in vitro*. Moreover, there was no antibody available to isolate ephrinB2$^+$ ECs from tumors using a cell sorter. Therefore, we used SVEC, an EC line, stably and strongly induced with ephrinB2.

Thus far, a variety of functions of Eph receptors and their ephrin ligands have been reported in the areas of cell migration, repulsion, and adhesion (5, 6, 8, 31, 32). Although it has been proposed that this receptor/ligand system is not involved in cell proliferation, nevertheless, it has also been reported that ephrin-A/EphA receptor signaling plays a key role in controlling the size of the mouse cerebral cortex by regulating cortical progenitor cell apoptosis (33). Moreover, we previously reported that EphB4 reverse signaling via ephrinB2 inhibited the mitotic activity of ephrinB2$^+$ ECs (25). Because of bidirectional signals termed forward signaling via EphB4 and reverse signaling via ephrinB2, we suggested that EphB4/ephrinB2 works on the arterial-venous interface through this bidirectional repulsion to form the arterial-venous boundary. However, in this report, we have clearly shown that reverse signaling via ephrinB2 led to the apoptosis of ephrinB2$^+$ cells (SVEC/ephrinB2), whereas forward signaling via EphB4 in tumor cells did not induce the apoptosis of EphB4$^+$ tumor cells (B16/EphB4). Taken together, this suggested that reverse signaling via ephrinB2 in ECs might terminate arteriogenesis during angiogenesis or induce regression of newly developed arterial blood vessels.

The function of EphB4/ephrinB2 in the development of blood vessel formation during embryogenesis has been the focus of research (2–4). In addition, its role in tumor angiogenesis has also been examined by a variety of methods, such as systemic or local administration of soluble EphB4 receptors (34, 35), site-specific expression of EphB4 or kinase-dead EphB4 in ECs retrovirally (36), and a xenograft model using breast cancer cells expressing kinase-dead EphB4 receptor (37). In the case of soluble EphB4 administration, tumor angiogenesis was perturbed (34, 35). This effect might result from the suppression of forward and reverse signaling via EphB4 and ephrinB2, respectively. Recently, the enhancement of EphB4 reverse signaling via ephrinB2 in ECs, in which EphB4 was ectopically induced in the ECs of tumors, has been reported to increase vascular density and permeability of blood vessels in tumors (36). These results indicated that EphB4/ephrinB2 signaling is active in tumor angiogenesis. However, the function of EphB4 in tumor cells for blood vessel formation has not been well clarified. One piece of research has shown that kinase-dead EphB4 expressed in tumor

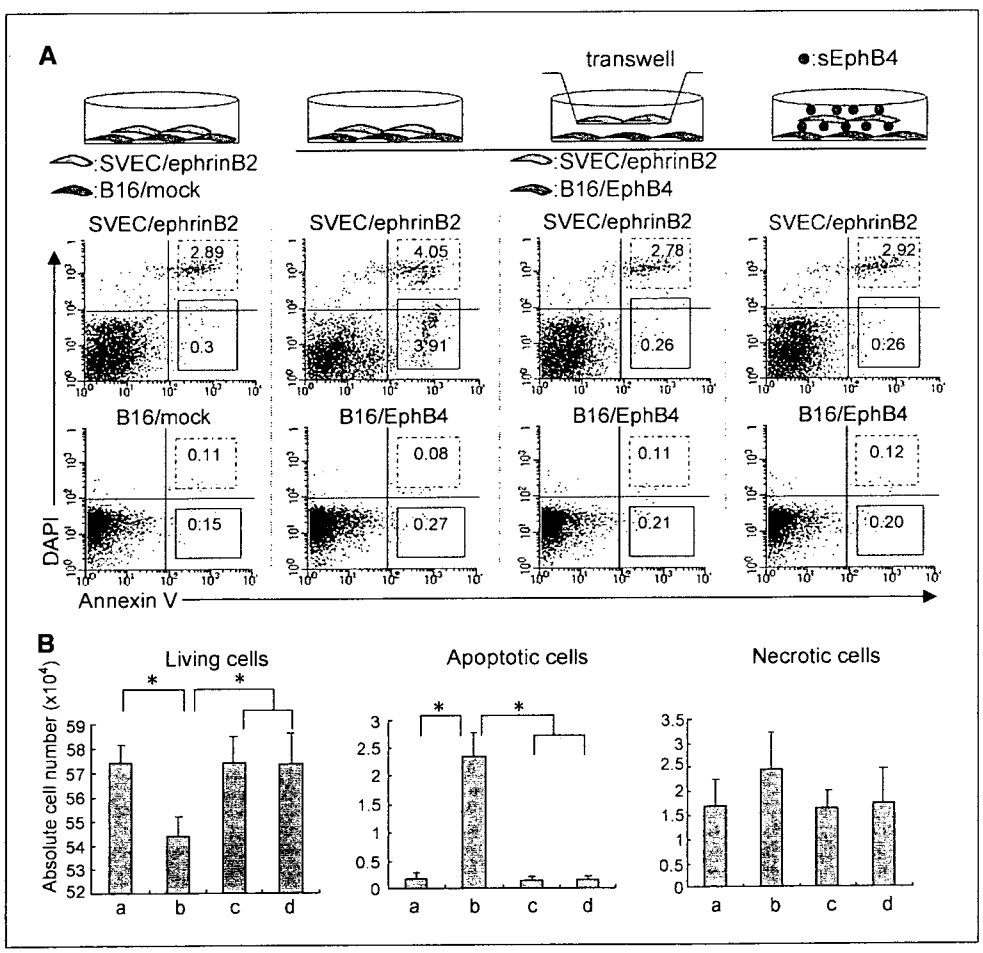

Figure 6. Effect of EphB4 overexpression in B16 cells on ephrinB2$^+$ SVECs as a reverse signaling via ephrinB2. *A, first* and *second columns*, direct coculture of SVEC/ephrinB2 cells with B16/mock or B16/EphB4 cells, respectively. *Third column*, indirect coculture of SVEC/ephrinB2 cells with B16/EphB4 cells separated with a transmembrane having 0.4-μm pores. *Fourth column*, direct coculture of SVEC/ephrinB2 cells with B16/EphB4 cells in the presence of soluble EphB4 (sEphB4). Schematic presentation of coculturing is presented on the top. B16 tumor cells or SVECs were prelabeled with PKH26 red fluorescence or PKH67 green fluorescence, respectively. After 24 h of coculture, cells gated by PKH67 or PKH26 discrimination (Supplementary Fig. S2) were analyzed by staining with anti-Annexin V-Cy5 and DAPI by FACS. Numbers in each quadrant indicate the percentage of Annexin V$^+$DAPI$^-$ apoptotic cells (*solid squares*) or Annexin V$^+$DAPI$^+$ dead cells (*dashed squares*) among the total cells. *B*, absolute number of living, apoptotic, or necrotic SVEC/ephrinB2 cells among the number of harvested whole cells in each culture condition as in *A*. *a* to *d*, culture conditions described in *A*: *a*, left; *b*, second; *c*, third; *d*, right. *, $P < 0.05$ ($n = 3$).

cells, in which only reverse signaling via ephrinB2 was enhanced, increased tumor angiogenesis and tumor growth (37). At first glance, there seems to be a discrepancy between these data and those presented here. However, in our experiment, wild-type EphB4 overexpression in B16 tumor cells, in which both forward signaling via EphB4 for tumor cells and reverse signaling via ephrinB2 for ECs cells were enhanced, suppressed the development of ephrinB2$^+$ blood vessels and resulted in the retardation of tumor growth. Therefore, this suggests that secondary inside-out signaling molecules from EphB4$^+$ tumor cells, through forward signaling via EphB4, may induce apoptosis of ephrinB2$^+$ cells with reverse signaling. Recently, it was reported in humans that EphB4 was expressed in human colonic crypts and in early colorectal cancer lesions and that EphB4 expression was lost in advanced colorectal tumors (15). This examination correlates with our data and suggests that, within tumors, the expression of EphB4 inhibits arteriogenesis whereas the loss of EphB4 permits the supply of oxygen and nutrients by establishing arterial-venous circulation.

Recently, it was reported that the expression level of EphB4 in human ovarian cancers is correlated with poor response to chemotherapy (19). Our results can offer two possible, complementary, explanations for this finding. From our study, it seems that EphB4 overexpression in tumor cells inhibits the organization of arterio-venous patterning in tumors, which could increase the difficulty anticancer drugs have in penetrating deep into tumor tissue, whereas, additionally, this overexpression has an inhibitory effect on rapid tumor growth. It is well known that blood vessels in tumors are disorganized compared with those observed in normal tissue, and permeability is relatively suppressed in the tumor environment. Recently, a new therapeutic concept has emerged whereby the artificially induced normalization of blood vessels in tumors could allow the penetration of anticancer drugs deep into the site of the tumors (38); normalization of arterial-venous patterning might be one such strategy for cancer therapy. In this study, we used a B16 mouse melanoma cell line to observe the function of EphB4 in ephrinB2$^+$ EC development precisely because of the lack of ephrinB2 expression in B16 cells. In humans, there are no published reports showing EphB4 expression in primary melanomas but several articles have indicated that most human melanoma cell lines express EphB4 (14, 39). However, although coexpression of EphB4/ephrinB2 in human melanoma tissue samples or melanoma cell lines has not been reported, in both settings the expression level of ephrinB2 has been reported to vary, and it has been proposed that expression level correlates with malignancy (14, 40). The functions of ephrinB2 and EphB4 in melanomas seem to be redundant for tumorigenesis in which ephrinB2 and EphB4 are associated with both tumor cell viability and generation of microenvironment. To further clarify the function of the EphB4/ephrinB2 system, it will be necessary to examine how EphB4 and ephrinB2 expression in tumor cells is regulated during the ontogeny of tumors.

Acknowledgments

Received 2/7/2007; revised 6/15/2007; accepted 7/29/2007.

Grant support: Grant-in-Aid from The Ministry of Education, Culture, Sports, Science, and Technology of Japan (N. Takakura).

The costs of publication of this article were defrayed in part by the payment of page charges. This article must therefore be hereby marked *advertisement* in accordance with 18 U.S.C. Section 1734 solely to indicate this fact.

We thank N. Fujimoto for preparation of plasmid DNA and K. Fukuhara for administrative assistance.

References

1. Risau W. Mechanisms of angiogenesis. Nature 1997; 386:671–4.
2. Wang HU, Chen ZF, Anderson DJ. Molecular distinction and angiogenic interaction between embryonic arteries and veins revealed by ephrinB2 and its receptor EphB4. Cell 1998;93:741–53.
3. Adams RH, Wilkinson GA, Weiss C, et al. Roles of ephrinB ligands and EphB receptors in cardiovascular development: demarcation of arterial/venous domains, vascular morphogenesis, and sprouting angiogenesis. Genes Dev 1999;13:295–306.
4. Gerety SS, Wang HU, Chen ZF, Anderson DJ. Symmetrical mutant phenotypes of the receptor EphB4 and its specific transmembrane ligand ephrin-B2 in cardiovascular development. Mol Cell 1999;4:403–14.
5. Kullander K, Klein R. Mechanisms and functions of Eph and ephrin signaling. Nat Rev Mol Cell Biol 2002;3: 475–86.
6. Mellitzer G, Xu Q, Wilkinson DG. Control of cell behaviour by signalling through Eph receptors and ephrins. Curr Opin Neurobiol 2000;10:400–8.
7. Gale NW, Baluk P, Pan L, et al. Ephrin-B2 selectively marks arterial vessels and neovascularization sites in the adult, with expression in both endothelial and smooth-muscle cells. Dev Biol 2001;230:151–60.
8. Wilkinson DG. Multiple roles of EPH receptors and ephrins in neural development. Nat Rev Neurosci 2001;2: 155–64.
9. Knoll B, Drescher U. Ephrin-As as receptors in topographic projections. Trends Neurosci 2002;25:145–9.
10. Barrios A, Poole RJ, Durbin L, Brennan C, Holder N, Wilson SW. Eph/Ephrin signaling regulates the mesenchymal-to-epithelial transition of the paraxial mesoderm during somite morphogenesis. Curr Biol 2003;13: 1571–82.
11. Adams RH. Vascular patterning by Eph receptor tyrosine kinases and ephrins. Semin Cell Dev Biol 2002; 13:55–60.
12. Adams RH, Klein R. Eph receptors and ephrin ligands: essential mediators of vascular development. Trends Cardiovasc Med 2000;10:183–8.
13. Adams RH, Diella F, Hennig S, Helmbacher F, Deutsch U, Klein R. The cytoplasmic domain of the ligand ephrinB2 is required for vascular morphogenesis but not cranial neural crest migration. Cell 2001;104: 57–69.
14. Nakamoto M, Bergemann AD. Diverse roles for the Eph family of receptor tyrosine kinases in carcinogenesis. Microsc Res Tech 2002;59:58–67.
15. Batlle E, Bacani J, Begthel H, et al. EphB receptor activity suppresses colorectal cancer progression. Nature 2005;435:1126–30.
16. Liu W, Ahmad SA, Jung YD, et al. Coexpression of ephrin-Bs and their receptors in colon carcinoma. Cancer 2002;94:934–9.
17. Xia G, Kumar SR, Masood R, et al. Up-regulation of EphB4 in mesothelioma and its biological significance. Clin Cancer Res 2005;11:4305–15.
18. Xia G, Kumar SR, Stein JP, et al. EphB4 receptor tyrosine kinase is expressed in bladder cancer and provides signals for cell survival. Oncogene 2006;25: 769–80.
19. Wu Q, Suo Z, Kristensen GB, Baekelandt M, Nesland JM. The prognostic impact of EphB2/B4 expression on patients with advanced ovarian carcinoma. Gynecol Oncol 2006;102:15–21.
20. Berclaz G, Flutsch B, Altermatt HJ, et al. Loss of EphB4 receptor tyrosine kinase protein expression during carcinogenesis of the human breast. Oncol Rep 2002;9:985–9.
21. Masood R, Kumar SR, Sinha UK, et al. EphB4 provides survival advantage to squamous cell carcinoma of the head and neck. Int J Cancer 2006;119:1236–48.
22. Berclaz G, Karamitopoulou E, Mazzucchelli L, et al. Activation of the receptor protein tyrosine kinase EphB4 in endometrial hyperplasia and endometrial carcinoma. Ann Oncol 2003;14:220–6.
23. Takai N, Miyazaki T, Fujisawa K, Nasu K, Miyakawa I. Expression of receptor tyrosine kinase EphB4 and its ligand ephrin-B2 is associated with malignant potential in endometrial cancer. Oncol Rep 2001;8:567–73.
24. Tang XX, Brodeur GM, Campling BG, Ikegaki N. Coexpression of transcripts encoding EPHB receptor protein tyrosine kinases and their ephrin-B ligands in human small cell lung carcinoma. Clin Cancer Res 1999; 5:455–60.
25. Sorokin L, Girg W, Gopfert T, Hallmann R, Deutzmann R. Expression of novel 400-kDa laminin chains by mouse and bovine endothelial cells. Eur J Biochem 1994;223:603–10.
26. Zhang XQ, Takakura N, Oike Y, et al. Stromal cells expressing ephrin-B2 promote the growth and sprouting of ephrin-B2(+) endothelial cells. Blood 2001;98: 1028–37.
27. Takakura N, Yoshida H, Ogura Y, Kataoka H, Nishikawa S, Nishikawa S. PDGFRα expression during mouse embryogenesis: immunolocalization analyzed by whole-mount immunohistostaining using the monoclonal anti-mouse PDGFRα antibody APA5. J Histochem Cytochem 1997;45:883–93.
28. Takakura N, Watanabe T, Suenobu S, et al. A role for hematopoietic stem cells in promoting angiogenesis. Cell 2000;102:199–209.

29. Takakura N, Huang XL, Naruse T, et al. Critical role of the TIE2 endothelial cell receptor in the development of definitive hematopoiesis. Immunity 1998;9: 677–86.
30. Okamoto R, Ueno M, Yamada Y, et al. Hematopoietic cells regulate the angiogenic switch during tumorigenesis. Blood 2005;105:2757–63.
31. Holmberg J, Clarke DL, Frisen J. Regulation of repulsion versus adhesion by different splice forms of an Eph receptor. Nature 2000;408:203–6.
32. Cowan CA, Henkemeyer M. Ephrins in reverse, park and drive. Trends Cell Biol 2002;12:339–46.
33. Depaepe V, Suarez-Gonzalez N, Dufour A, et al. Ephrin signalling controls brain size by regulating apoptosis of neural progenitors. Nature 2005;435: 1244–50.
34. Kertesz N, Krasnoperov V, Reddy R, et al. The soluble extracellular domain of EphB4 (sEphB4) antagonizes EphB4-2 interaction, modulates angiogenesis, and inhibits tumor growth. Blood 2006;107:2330–8.
35. Martiny-Baron G, Korff T, Schaffner F, et al. Inhibition of tumor growth and angiogenesis by soluble EphB4. Neoplasia 2004;6:248–57.
36. Erber R, Eichelsbacher U, Powajbo V, et al. EphB4 controls blood vascular morphogenesis during postnatal angiogenesis. EMBO J 2006;25:628–41.
37. Noren NK, Lu M, Freeman AL, Koolpe M, Pasquale EB. Interplay between EphB4 on tumor cells and vascular ephrin-B2 regulates tumor growth. Proc Natl Acad Sci U S A 2004;101:5583–8.
38. Jain RK. Normalization of tumor vasculature: an emerging concept in antiangiogenic therapy. Science 2005;307:58–62.
39. Bennett BD, Wang Z, Kuang WJ, et al. Cloning and characterization of HTK, a novel transmembrane tyrosine kinase of the EPH subfamily. J Biol Chem 1994;269: 14211–8.
40. Vogt T, Stolz W, Welsh J, et al. Overexpression of Lerk-5/Eplg5 messenger RNA: a novel marker for increased tumorigenicity and metastatic potential in human malignant melanomas. Clin Cancer Res 1998;4: 791–7.

STEM CELLS

TISSUE-SPECIFIC STEM CELLS

Cardiac Stem Cells in Brown Adipose Tissue Express CD133 and Induce Bone Marrow Nonhematopoietic Cells to Differentiate into Cardiomyocytes

YOSHIHIRO YAMADA,[a,b,c] SHIN-ICHIRO YOKOYAMA,[d] XIANG-DI WANG,[b] NOBORU FUKUDA,[d] NOBUYUKI TAKAKURA[a,b,c]

[a]Department of Signal Transduction, Research Institute for Microbial Diseases, Osaka University, Osaka, Japan; [b]Department of Stem Cell Biology, Cancer Research Institute of Kanazawa University, Kanazawa, Japan; [c]PREST, Japan Science and Technology Agency, Saitama, Japan; [d]Second Department of Internal Medicine, Nihon University School of Medicine, Tokyo, Japan

Key Words. AC133 • Adult bone marrow • Myogenesis • Adipogenesis

ABSTRACT

Recently, there has been noteworthy progress in the field of cardiac regeneration therapy. We previously reported that brown adipose tissue (BAT) contained cardiac progenitor cells that were relevant to the regeneration of damaged myocardium. In this study, we found that CD133-positive, but not c-Kit- or Sca-1-positive, cells in BAT differentiated into cardiomyocytes (CMs) with a high frequency. Moreover, we found that CD133$^+$ brown adipose tissue-derived cells (BATDCs) effectively induced bone marrow cells (BMCs) into CMs. BMCs are considered to have the greatest potential as a source of CMs, and two sorts of stem cell populations, the MSCs and hematopoietic stem cells (HSCs), have been reported to differentiate into CMs; however, it has not been determined which population is a better source of CMs. Here we show that CD133-positive BATDCs induce BMCs into CMs, not through cell fusion but through bivalent cation-mediated cell-to-cell contact when cocultured. Moreover, BMCs induced by BATDCs are able to act as CM repletion in an in vivo infarction model. Finally, we found that CD45$^-$CD31$^-$ CD105$^+$ nonhematopoietic cells, when cocultured with BATDCs, generated more than 20 times the number of CMs compared with lin$^-$c-Kit$^+$ HSCs. Taken together, these data suggest that CD133-positive BATDCs are a useful tool as CM inducers, as well as a source of CMs, and that the nonhematopoietic fraction in bone marrow is also a major source of CMs. STEM CELLS *2007;25:1326–1333*

Disclosure of potential conflicts of interest is found at the end of this article.

INTRODUCTION

Cell transplantation and gene transfer are two of the foremost therapies with potential for regenerating damaged cardiomyocytes (CMs) and enabling revascularization. Embryonic stem cells, skeletal myoblasts, and c-kit- or Sca-1-positive cardiac stem cells (CSCs) in heart tissue have all been reported as candidates for the replacement of CMs; however, each is associated with problems, including those involving allergenic, etiologic, and arrhythmic issues.

Bone marrow cells (BMCs) are a well-known source of various kinds of stem cells. BMCs can contribute to the regeneration of various tissues, and their clinical application is easier than that of other candidates. Recent studies have suggested that CMs might also originate from BMCs, which are composed of at least two cell populations. Among these are hematopoietic cells (HCs) [1, 2] and mesenchymal cells [3–5], both of which have been suggested as sources of CMs. Nevertheless, the ability of the former to differentiate into CMs is by no means clear. Several studies have demonstrated that hematopoietic stem cells (HSCs) can induce myogenic repair by their capacity to differentiate into CMs [1, 2]. However, two other studies, which used an in vivo infarction model, reported that HSCs were incapable of differentiating into CMs [6, 7]. Moreover, Alvarez-Dolado et al. demonstrated that bone marrow (BM)-derived CMs were observed at low frequency and were generated by cell fusion with donor CD45$^+$ HCs [8]. Taken together, the results from these various studies suggest that it remains to be resolved whether plasticity of HSCs truly occurs and which population will prove to be the best source for the repair of damaged cardiac tissue. Moreover, specific molecular cues for the differentiation of CMs from BMCs have not been identified. This lack of knowledge means that, at present, it is difficult to effectively induce immature cells into CMs.

In this study, we show that CD133 is a CSC marker in brown adipose tissue-derived cells (BATDCs), which had been identified previously as a source of CSCs [9]. CD133 was first isolated from neuroepithelial stem cells as mouse Prominin-1 [10]; subsequently, it was reported that CD34$^+$ HSCs isolated from fetal liver, BM, and cord blood expressed CD133 (AC133) [11]. Moreover, CD133 antigen expression was detected in

Correspondence: Nobuyuki Takakura, M.D., Ph.D., Department of Signal Transduction, Research Institute for Microbial Diseases, Osaka University, 3-1 Yamadaoka, Suita-shi, Osaka 565-0871, Japan. Telephone: 81-6-6879-8316; Fax: 81-6-6879-8314; e-mail: ntakaku@biken.osaka-u.ac.jp; Yoshihiro Yamada, M.D., Ph.D., Department of Signal Transduction, Research Institute for Microbial Diseases, Osaka University, 3-1 Yamadaoka, Suita-shi, Osaka 565-0871, Japan. Telephone: 81-6-6879-8316; Fax: 81-6-6879-8314; e-mail: yamaday@biken.osaka-u.ac.jp Received September 19, 2006; accepted for publication January 30, 2007; first published online in STEM CELLS *EXPRESS* February 8, 2007. 1066-5099/2007/$30.00/0 doi: 10.1634/stemcells.2006-0588

undifferentiated cells, including endothelial progenitor cells [12], fetal brain stem cells [13], embryonic epithelium [14], prostatic epithelial stem cells [15], myogenic cells [16], and certain cancer stem cells, such as retinoblastoma [17] and medulloblastoma [18]. These results indicated that CD133 might be an antigen common to several stem cells, including CSCs, in brown adipose tissue (BAT). Second, we have shown that BMCs could differentiate with high efficiency into CMs by coculturing with BATDCs. In this induction system, we have demonstrated that bivalent cation-mediated cell-to-cell contact was critical for the differentiation of BMCs into CMs, and we have also investigated cadherin-mediated cell contact. Finally, we have demonstrated that in the bone marrow (BM) population, $CD45^-CD31^-CD105^+$ non-HCs could effectively differentiate into CMs, in contrast to the $lin^-c\text{-}Kit^+$ HSCs.

MATERIALS AND METHODS

Cell Preparation and Flow Cytometry

BAT was dissected from the interscapular region of postnatal day 1 (P1) to P7 neonates of C57BL/6 mice. BAT was dissociated by Dispasell (Roche Diagnostics, Mannheim, Germany, http://www.roche-applied-science.com), drawn through a 23-gauge needle, and prepared as a single-cell suspension, as previously reported [9]. BMCs were harvested from femurs and tibias of green fluorescent protein (GFP) transgenic mice (green mice) as previously described [19]. The cell-staining procedure for the flow cytometry was also as previously described [20]. The monoclonal antibodies (mAbs) used in immunofluorescence staining were anti-CD45, -ter119, -CD31, -CD29, -c-kit, -Sca1, -CD105, and -CD133 mAbs (BD Pharmingen, San Diego, http://www.bdbiosciences.com/pharmingen). All mAbs were purified and conjugated with fluorescein isothiocyanate, phycoerythrin (PE), biotin, or allophycocyanin (APC). Biotinylated antibodies were visualized with PE-conjugated streptavidin (BD Pharmingen) or APC-conjugated streptavidin (BD Pharmingen). Cells were incubated for 5 minutes on ice with CD16/32 (FcγIII/II Receptor) (1:100) (Fcblock; BD Pharmingen) prior to staining with primary antibody. Cells were incubated in 5% fetal calf serum (FCS)/phosphate-buffered saline (PBS) (washing buffer) with primary antibody for 30 minutes on ice and washed twice with washing buffer. Secondary antibody was added, and the cells were incubated for 30 minutes on ice. After incubation, cells were washed twice with, and suspended in, the washing buffer for fluorescence-activated cell sorting (FACS) analysis. The stained cells were analyzed and sorted with an EPICS flow cytometer (Beckman Coulter, San Jose, CA, http://www.beckmancoulter.com). The sorted cells were added to 24-well dishes (Nunc, Roskilde, Denmark, http://www.nuncbrand.com), precoated with 0.1% gelatin (Sigma-Aldrich, St. Louis, http://www.sigmaaldrich.com), and cultured in Dulbecco's modified Eagle's medium (DMEM) supplemented with 10% FCS and 10^{-5} M 2-mercaptoethanol at 37°C in a 5% CO_2 incubator.

Immunohistochemistry

Immunohistochemical analyses of tissue sections and culture dishes and the tissue fixation procedure were performed as previously described [9, 20]. The fixed specimens were embedded in Optimum Cutting Temperature (OCT) compound (Sakura Finetechnical, Tokyo, http://www.sakuraus.com) and sectioned at 7 μm. Anti-sarcomeric actin (anti-SA) (clone 5C5; Sigma-Aldrich), anti-GATA-4 (Santa Cruz Biotechnology Inc., Santa Cruz, CA, http://www.scbt.com), -MEF2C (Cell Signaling Technology, Beverly, MA, http://www.cellsignal.com), -connexin43 (Sigma-Aldrich), -atrial natriuretic factor (ANF) (Santa Cruz Biotechnology), and -GFP antibodies (Santa Cruz Biotechnology) for tissue sections, and anti-SA, -cardiac troponin T (Santa Cruz Biotechnology), -cardiac troponin I (clone 13–11; Neomarkers, Fremont, CA, http://www.labvision.com) [21–23], -GATA-4, -MEF2C, and -pan-cadherin (Sigma-Aldrich) antibodies for CM culture dishes were used in this assay. In brief, anti-SA was developed with Alexa Fluor 488-, 546-, or 633-conjugated goat anti-mouse IgM (Molecular Probes Inc., Eugene, OR, http://probes.invitrogen.com); anti-pan-cadherin was developed with 546-conjugated goat anti-mouse IgG (Molecular Probes); and anti-cardiac troponin T, cardiac troponin I, -MEF2C, -GATA-4, -connexin43, and -ANF antibodies were developed with Alexa Fluor 488-, 546-, or 633-conjugated goat anti-rabbit IgG (Molecular Probes). Nuclear staining was performed with 4,6-diamidino-2-phenylindole or TOPRO3 (Molecular Probes). Finally, the sections and dishes were observed using an Olympus IX-70 microscope equipped with UPlanFI 4/0.13 and LCPlanFI 20/0.04 dry objective lenses (Olympus, Tokyo, http://www.olympus-global.com). Images were acquired with a CoolSnap digital camera (Roper Scientific, Tokyo, http://www.roperscientific.com). In all assays, an isotype-matched control Ig was used as a negative control, and it was confirmed that the positive signals were not derived from nonspecific background. Images were processed using Adobe Photoshop 7.0 software (Adobe Systems Inc., San Jose, CA, http://www.abode.com).

Transmission Electron Microscopy

Cells were washed in phosphate buffer and fixed with 2% glutaraldehyde and 1% paraformaldehyde in PBS. Samples were post-fixed with 1% osmium in PBS, rinsed, dehydrated, and embedded in araldite (DAKO, Glostrup, Denmark, http://www.dako.com). Then, samples were cut with a diamond knife and examined under a Jeol 100CX (Tokyo, http://www.jeol.co.jp) electron microscope.

Cell Coculture

BATDCs and BMCs were prepared as described above. In situations where $CD133^+$ BATDCs and BMCs were cocultured in contact conditions, 2×10^4 $CD133^+$ BATDCs were plated per well of a 24-well plate and cultured for 10 days before being fixed with 0.5% paraformaldehyde for 15 minutes at room temperature. Fixed cells were washed extensively, first with PBS and then with DMEM/10% FCS. After washing, 1×10^5 BM mononuclear cells (BMMNCs), 1×10^4 $lin^-c\text{-}Kit^+$ HSCs, or 1×10^4 $CD45^-ter119^-CD31^-CD105^+$ MSCs from GFP mice were cultured with fixed BATDCs, as described above, for 10 days and then stained with anti-SA (Sigma-Aldrich), -GATA-4 (Santa Cruz Biotechnology), -MEF-2C (Cell Signaling Technology), and -GFP (MBL International Corp., Nagoya, Japan, http://www.mblintl.com) antibodies. Under separate conditions, $CD133^+$ BATDCs from ROSA26 mice were cocultured on 0.4-μm cell culture inserts (Becton, Dickinson and Company, San Jose, CA, http://www.bd.com) with BMMNCs from green mice in 0.1% gelatin-coated dishes (Becton Dickinson) for 14 days and then stained with anti-SA (Sigma-Aldrich) and anti-GATA-4 (Santa Cruz Biotechnology).

To analyze the diverse signaling between BATDCs and BM-derived cells, we used an anti-E-cadherin antibody (ECCD-1; Calbiochem, La Jolla, CA, http://www.emdbiosciences.com), E-cadherin-Fc, N-cadherin-Fc, and R-cadherin-Fc (all purchased from R&D Systems Inc., Minneapolis, http://www.rndsystems.com).

Reverse Transcription-Polymerase Chain Reaction Analysis

The RNeasy Mini kit (Qiagen, Hilden, Germany, http://www1.qiagen.com) was used for isolation of total RNA from BAT and BMCs. Total RNA was reverse transcribed using the reverse transcription-polymerase chain reaction (RT-PCR) kit (Clontech, Palo Alto, CA, http://www.clontech.com). The cDNA was amplified using Advantage Polymerase Mix (Clontech) in a GeneAmp PCR system, model 9700 (PerkinElmer Life and Analytical Sciences, Norwalk, CT, http://www.perkinelmer.com), by 40–50 cycles. The sequences of the gene-specific primers for RT-PCR were as follows: 5′-α-myosin heavy chain (MHC), TGTCTGCTCTCCACCGGGAAAATCT; 3′-α-MHC, CATGGCCAATTCTTGACTCCCATGA; 5′-β-MHC, AACCCACCCAAGTTCGACAAG ATCG; 3′-β-MHC, CCAACTTTCCTGTTGCCCCAAAAATG; 5′-α-skeletal actin, GGAGATTGTGCGCGACATCAAAGAG; 3′-α-skeletal actin, CTGGTTCCTCCAATGGGATATCTTC; 5′-α-cardiac actin, TGTGTTACGTCGCCCTGGATTTTGA; 3′-α-cardiac actin, TTGCTGATCCACATTT

GCTGGAAGG; 5′-myosin light chain (MLC)-2a, AGCAGGCA-CAACGTGGCTCTTCTAA; 3′-MLC-2a, CCTGGGTCAT-GAGAAGCTGCTTGAA; 5′-MLC-2v, ATGGCACCTTTGTTTGC-CAAGAAGC; 3′-MLC-2v, CCCTCGGGATCAAACACCTTAATG; 5′-GATA4, GAGTGAGTCAATTGTGGGGCCATGT; 3′-GATA4, TGCTGCTAGTGGCA TTGCTGGAGTT; 5′-glyceraldehyde-3-phosphate dehydrogenase (G3PDH), TGAAGGTCGGTGT-GAACGGATTTGGC; 3′-G3PDH, CATGTAGGCCATGAG GTC-CACCAC; 5′-lacZ, GCGTTACCCAACTTAATCG; 3′-lacZ, TGTGAGCGAGTAACAACC; 5′-GFP, TACGGCAAGCTGAC-CCTGAA; 3′-GFP, TGTGATCGCGCTTCTCGTTG. Each cycle consisted of denaturation at 94°C for 30 seconds and annealing/extension at 70°C for 4 minutes except lacZ and GFP. For lacZ and GFP, each cycle consisted of denaturation at 94°C for 30 second, annealing at 60°C for 1 minute, and extension 72°C for 1 minute.

Myocardial Infarction and Cell Implantation and Echocardiography

BMCs derived from GFP transgenic Sprague-Dawley rats [24] at 2 months old were cocultured for 5 days with CD133$^+$ BATDCs taken from wild-type Sprague-Dawley rats at 3 days, and then the GFP-positive fraction was sorted using an EPICS flow cytometer and implanted into the heart. Myocardial infarctions (MIs) were induced in female Sprague-Dawley rats at 2 months of age as described previously [9]. After verifying the MIs, 10 rats were injected with 2×10^5 cells each, in five opposite regions bordering the infarct, and then sacrificed after 30 days. At each time interval, sham-operated rats were injected with saline as controls. Under ketamine (Dainippon Pharmaceutical, Osaka, Japan, http://www.ds-pharma.co.jp) anesthesia, echocardiography was performed at 29 days. From M mode tracings, left ventriculus end-diastolic and systolic diameter and wall thickness were obtained, and then the percentage of fractional shortening was calculated. Echocardiographic acquisition and analysis were performed by an echocardiographer blinded to treatment group. Results represent the mean of five separate experiments. Mortality was lower, but not significantly different, in the treated rats, averaging 35% in all groups. Protocols were approved by the institutional review board.

Fluorescence In Situ Hybridization Staining

After staining of CMs with anti-SA antibody as described above, we performed fluorescence in situ hybridization (FISH) to determine the presence of rat X and Y chromosomes (Cambio, Cambridge, U.K., http://www.cambio.co.uk) according to the manufacturer's instructions. A digestion with proteinase K (DAKO) (20 μg/ml at 37°C, 5 minutes) was added at the beginning of the FISH protocol. Nuclear staining was performed with TOPRO3 (Molecular Probes). Pictures were taken by confocal microscope (LSM510; Carl Zeiss MicroImaging, Inc., Göttingen, Germany, http://www.zeiss.com).

RESULTS

Surface Phenotype of CM Progenitors in BAT

A putative stem cell population has recently been identified in adipose tissue [25]. This cell population expressed multiple CD marker antigens, such as CD29, CD44, CD90, and CD105, similar to those observed on MSCs. We previously reported that BATDCs included cells that are able to differentiate into CMs [9], and another group has demonstrated the capacity of adipose tissue-derived mesenchymal cells to differentiate into CMs [26]. Other reports have indicated that cardiac progenitor cells in the adult heart expressed c-Kit and Sca-1, which were first established as HSC markers [21, 27]. Therefore, using flow cytometric analysis, we analyzed several stem cell markers and multiple CD markers on cells from BATDCs, which can differentiate into CMs. First, we checked for ter119 (erythrocyte marker), CD45 (LCA) (panleukocyte marker), and CD31 (endothelial marker). Among CD45$^-$ter119$^-$CD31$^-$ cells (nonhematopoietic, nonendothelial cells), c-Kit, Sca-1, and CD133 expression was observed on 1.4%, 16.6%, and 3.5% of total BATDCs, respectively (Fig. 1A). To clarify which populations have a high potential to produce CMs, we cultured a CD45$^-$ter119$^-$CD31$^-$ subpopulation fractionated by c-Kit, Sca-1, or CD133 expression. Among them, CD133-positive BATDCs differentiated into CMs with a higher incidence compared with cells in other fractions and CD29-positive (CD45$^-$ter119$^-$CD31$^-$) cells, which we had previously reported as a CM-enriched population (Fig. 1C). Indeed, approximately 50% of adherent cells from cultured CD133-positive cells among CD45$^-$ter119$^-$CD31$^-$ cells differentiated into SA$^+$GATA-4$^+$ (Fig. 1B, a and b, 1C, a and b), cardiac-troponin T$^+$GATA-4$^+$ (Fig. 1B, c and d), and cardiac-troponin I$^+$MEF2C$^+$ (Fig. 1B, e and f). Furthermore, electron microscopic analysis indicated that these cells had cellular structures typical of CMs, such as an organized sarcomere with typical cross-strain, developed Z-bands, long mitochondria in the cytoplasm, and centrally positioned nuclei (Fig. 1B, g). To provide additional evidence that CD133$^+$ BATDCs have the phenotype of CMs, we performed pharmacological studies (supplemental online data). The calcium antagonist verapamil slowed the beating rate, and the β-agonist isoproterenol induced a dose-dependent increase of the spontaneous contraction rate; however, the β-adrenergic antagonist propranolol reversed the isoproterenol-induced acceleration. These results also indicated that CD133$^+$ BATDCs have the functional character of CMs.

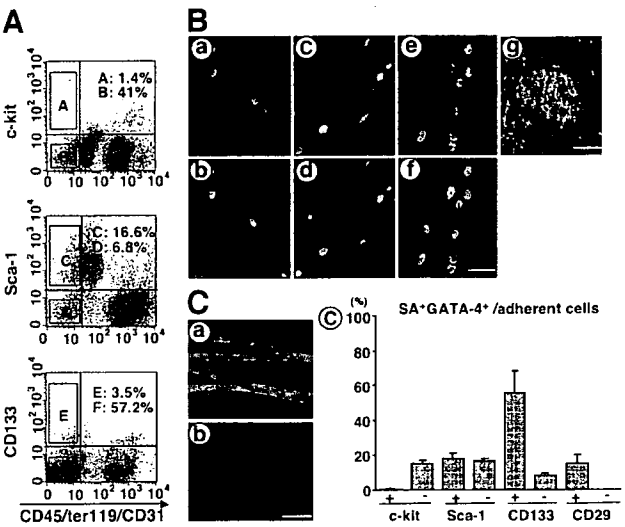

Figure 1. Phenotype of cardiomyocyte (CM) stem cells in brown adipose tissue (BAT). **(A):** Cells derived from BAT were stained with a mixture of anti-CD45, -ter119, and -CD31 antibodies (*x*-axis) and anti-c-Kit, -Sca-1 or -CD133 antibody (*y*-axis). **(B):** Immunocytochemical analysis and transmission electromicrograph of CMs derived from CD133$^+$ (CD45$^-$ter119$^-$CD31$^-$) BATDCs. CD133-positive cells generated SA$^+$ (red)/GATA-4$^+$ (green) cells (a), cardiac troponin T$^+$ (red)/GATA-4$^+$ (green) cells (c), or cardiac troponin I$^+$ (red)/MEF2C$^+$ (green) cells (e). Nuclear staining by TOPRO3 in a, c, and e is shown in b, d, and f, respectively. Notably, well-organized sarcomeres, Z-band, and a large number of mitochondria were observed in CD133$^+$ BATDCs. Scale bar = 10 μm (f) and 1 μm (g). **(C):** a, Existence of SA-positive (green) and GATA4-positive (red) CMs in the culture of CD133+ BATDCs. b, Nuclear staining with 4,6-diamidino-2-phenylindole in the same field as shown in panel a. Note that this low-power field view clearly showed that approximately 50% of adherent cells are CMs. Scale bar = 20 μm. c, Quantitative evaluation of differentiation potential for CMs from each fraction of BATDCs as indicated. The same number of cells (1×10^4) of each fraction was cultured. Note that c-Kit$^+$ (CD45$^-$ter119$^-$CD31$^-$) cells could not differentiate into CMs, and CD133$^+$ (CD45$^-$ter119$^-$CD31$^-$) cells were the most effective at differentiating into CMs.

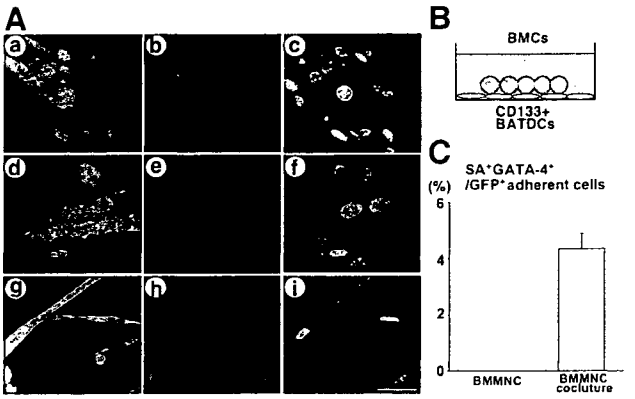

Figure 2. BMMNCs can differentiate into cardiomyocytes (CMs) upon coculturing with BATDCs. **(A):** Immunocytochemical analysis of BMMNCs from green mice cocultured for 14 days with CD133-positive BATDCs from wild-type mice. a–c, GFP (green) (a), GATA-4 (red) (b), and nuclear staining with TOPRO3 (blue) merged with that shown in b (c). d–f, GFP (green) (d), MEF2C (red) (e), and nuclear staining with TOPRO3 (blue) merged with that shown in e (f). g–I, GFP (green) (g), SA (red) (h), and GATA-4 (blue) merged with that shown in h (i). Scale bar = 5 μm (i). **(B):** Schematic presentation of coculturing BMMNCs from green mice with CD133-positive BATDCs from wild-type mice. **(C):** Quantitative evaluation of differentiated SA- and GATA4-positive CMs among adhering GFP-positive BM-derived cells. Data for BMMNC cocultured with CD133+ BATDCs and BMMNCs cultured alone are displayed. Results represent the mean of five independent experiments. Abbreviations: BATDC, brown adipose tissue-derived cell; BMC, bone marrow cell; BMMNC, bone marrow mononuclear cell; GFP, green fluorescent protein.

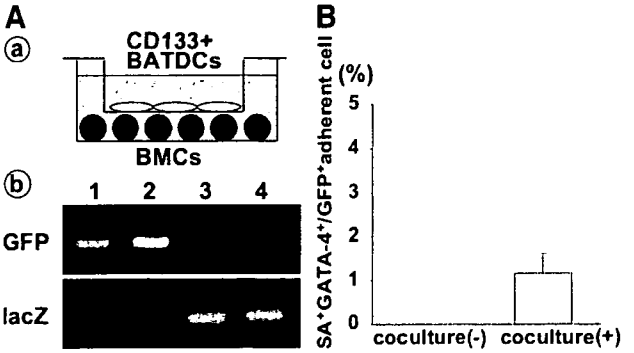

Figure 3. Bone marrow mononuclear cells (BMMNCs) differentiated into cardiomyocytes (CMs) in separated coculture system. **(A):** a, Schematic representation of the system for the separate coculture of BMMNCs with $CD133^+$ BATDCs. b, Reverse transcription-polymerase chain reaction analysis in separate culture conditions. BMMNCs were derived from green mice (lower chamber), and BATDCs were derived from ROSA26 mice (upper chamber). GFP signal was detected only in the lower chamber, and lacZ signal was detected only in the upper chamber. Lane 1, BMMNCs before culture (lower chamber); lane 2, BMMNCs after 14 days of culture (lower chamber); lane 3, BATDCs before culture; lane 4, BATDCs after 14 days of culture. **(B):** Quantitative evaluation of the differentiation potential for CMs from BMMNCs in separate culture conditions. Upon coculturing with BATDCs (coculture[+]), approximately 1.7% of adhering GFP-positive bone marrow cells differentiated into SA- and GATA4-positive CMs. CM development could not be observed when BMMNCs were cultured alone (coculture[−]). Results represent the mean of five independent experiments. Abbreviations: BATDC, brown adipose tissue-derived cell; BMC, bone marrow cell; GFP, green fluorescent protein.

BATDCs Effectively Induce CM Production from BMCs

A previous in vitro study showed that although BMCs were a source of CMs, they could not spontaneously differentiate into CMs; however, differentiation could be induced with 5-azacytidine, a DNA-hypomethylating agent [4]. It is thought that BMCs can differentiate into CMs upon adequate environmental molecular cues. As $CD133^+$ BATDCs differentiate into CMs spontaneously, this suggests that $CD133^+$ BATDCs produce molecules that induce the differentiation of $CD133^+$ BATDCs into CMs by an autocrine loop. Therefore, to test this ability, we cultured BMMNCs with BATDCs and observed whether or not, under these conditions, BMMNCs could differentiate into CMs. At first, $CD133^+$ cells were sorted from BAT by FACS and cultured on 0.1% gelatin-coated dishes. After 1 week, BMMNCs derived from green mice that express GFP ubiquitously in their tissues [28] were cocultured in direct contact with $CD133^+$ BATDCs, as shown in Figure 2B. By coculturing BMMNCs with CD133-positive BATDCs, nuclear-located GATA-4-positive (Fig. 2A, a–c), MEF2C-positive (Fig. 2A, d–f), and SA-positive (Fig. 2A, g–i) contracting cells were produced among the GFP-positive BMMNCs. However, the SA-positive and GATA-4-positive cells were not observed when BMMNCs were cultured alone under the same conditions (Fig. 2C).

BMMNCs with BATDCs Differentiated into CMs Without Fusion Mechanism

Recently, it has been suggested that cell fusion is the main mechanism that contributes to the development or maintenance of cardiac muscle and neuron regeneration [8, 29]. To exclude the possibility of cell fusion in our experiment, we cultured BMMNCs from green mice with BATDCs from ROSA26 mice, which express LacZ ubiquitously in their tissues, and separated the cells from these two different origins with a 0.4-μm-pore membrane (Fig. 3A, a). In this separating coculture system, $SA^+GATA\text{-}4^+$ CMs were also produced from BMMNCs when cocultured with BATDCs (Fig. 3B). Moreover, with PCR analysis, GFP-positive signals were detected only in the BMMNC layer, and lacZ-positive signals were detected only in the BATDCs layer from the cells before and after culturing (Fig. 3A, b). Therefore, we concluded that the development of CMs from BMMNCs was not dependent on cell fusion with BATDCs.

Cell Contact Mediated by Bivalent Cation Is Critical for the Differentiation of BMMNCs into CMs

We found that BMMNCs could differentiate into CMs under conditions in which the BMMNCs were cultured in direct or indirect contact with BATDCs; however, differentiation of BMMNCs into CMs was promoted more effectively by direct cell-to-cell contact between BMMNCs and BATDCs than under separated culture conditions (Figs. 2B, 3B). Indeed, 520 ± 40 versus 105 ± 18 SA^+GATA4^+ CMs were generated from 1×10^5 BMMNCs under direct and indirect cocultures, respectively. To exclude the possibility of cell fusion in the contact coculture system, we used paraformaldehyde-fixed cultured $CD133^+$ BATDCs, which cannot fuse with other cells but have an intact cell surface. After coculturing with fixed BATDCs, some GFP^+ BMMNC-derived cells (Fig. 4A, a) expressed cardiac-specific antigens, such as SA (Fig. 4A, b and c), GATA-4, and cardiac troponinT (data not shown). Moreover, these cells also had the typical features of CMs, confirmed by electron microscopic analysis (Fig. 4A, f).

Cadherin-mediated calcium-dependent cell-to-cell contact is widely believed to be involved in the regulation of the diverse signaling process for cell differentiation [30]. Therefore, we elucidated a potential role for calcium-dependent cell-to-cell contact in our coculture system. First, BMMNCs were incubated with the calcium chelator EDTA or EGTA on fixed BATDCs. This treatment abolished the adhesion of BMMNCs to fixed, differentiated BATDCs. By the suppression of cell adhesion of BMCs to differ-

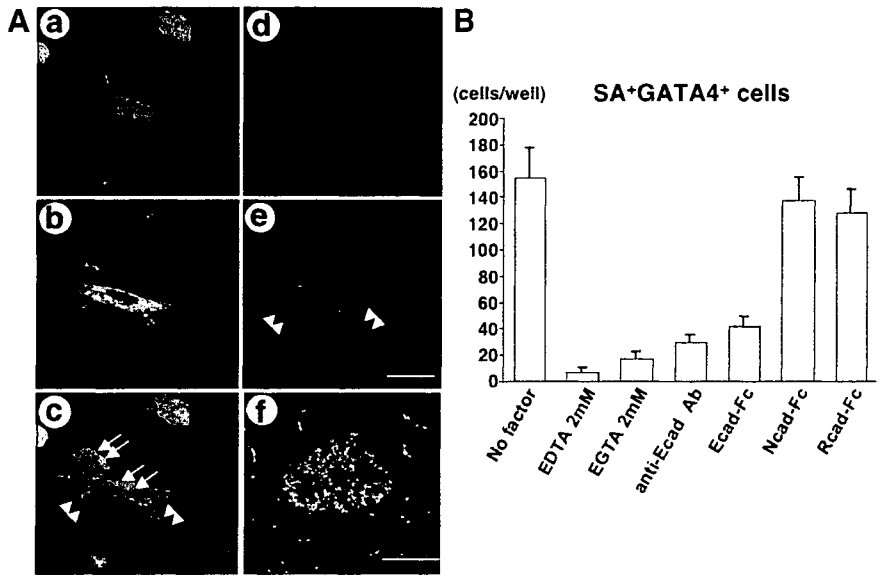

Figure 4. Differentiation of bone marrow mononuclear cells (BMMNCs) into cardiomyocytes (CMs) is mainly induced by bivalent cation-mediated cell contact with brown adipose tissue-derived cells (BATDCs). **(A):** Immunocytochemical staining of CMs from BMMNCs cocultured with fixed BATDCs for 14 days. Anti-GFP (green) (a and c), anti-SA(red) (d and e), and anti-pan-cadherin (blue) (b, c, and e) Abs were used in this assay. Arrows indicate SA^+GFP^+ cells interacting with SA^+GFP^- cells (arrowheads) through cadherin expression. f, Transmission electron micrographic analysis showed that BM-derived CMs had well-organized sarcomeres, Z-band, and a large number of mitochondria. Scale bar = 10 μm (e) and 1 μm (f). **(B):** Quantitative evaluation of differentiated CMs from BMMNCs in the presence or absence of EGTA, EDTA, or 100 μg/ml neutralizing Ab of Ecad, Ecad-Fc, Ncad-Fc, or Rcad-Fc when cocultured with fixed BATDCs. Adherent SA-positive and GATA-4-positive cells were counted in each culture condition. Results represent the mean of five independent experiments. Abbreviations: Ab, antibody; Ecad, E-cadherin; Ncad, N-cadherin; Rcad, R-cadherin.

entiated BATDCs (fixed), differentiation of BMCs into CMs was almost completely suppressed (Fig. 4B). Next, we examined which, out of E-cadherin (ECad), NCad, or RCad, was affected in this mechanism. We found that $CD133^+$ BATDCs abundantly expressed Ecad, and BMCs expressed Ecad and Ncad, as confirmed by PCR analysis (data not shown). To evaluate the effect of cadherins in this culture system, we added neutralizing antibody (Ab) against Ecad (anti-Ecad Ab) or soluble cadherin, such as Ecad-Fc, Ncad-Fc, or Rcad-Fc. Among these materials, anti-Ecad Ab and Ecad-Fc effectively inhibited the differentiation of BMMNCs into CMs. Taken together, these data suggest that Ecad-mediated cell-to-cell contact is important for the differentiation of BMMNCs into CMs.

Educated BMMNCs Contributed to CM Regeneration

The data above clearly indicate that CD133-positive BATDCs effectively induced CM production from BMCs. Next, we evaluated the length of time required for BMMNCs to become committed to CM lineage when cultured with BATDCs. For this purpose, we attempted to coculture BMMNCs from green rats expressing GFP with BATDCs for 1 to 10 days and harvested GFP-positive cells at intervals from the culture. GFP-positive cells were then sorted and cultured alone for an additional 14 days (Fig. 5A, a). In this experiment, we found that 5 days was enough for commitment of BMMNCs into CM lineage. Sorted GFP-positive cells did not express SA and GATA-4 (data not shown); however, they started to display contractile activity after 7 days of culturing. After 14 days of culturing, we found that approximately 10% of GFP-positive adherent cells differentiated into SA-positive and MEF2C-positive cells (Fig. 5A, b–d). To examine cardiac-specific genes and transcription factors in detail, we performed RT-PCR analysis and revealed that the expression of α-MHC, β-MHC, α-skeletal actin, α-cardiac actin, MLC-2v, and GATA4 was detected (Fig. 5A, e). Interestingly, this phenotype was similar to that of CMs derived from BATDCs [9].

Next, to determine whether BMMNCs exposed to BATDCs could effectively contribute to the regeneration of the heart, we injected the exposed BMMNCs into the hearts of rats after the induction of an acute MI. At first, we cocultured GFP-positive BMMNCs with CD133-positive BATDCs for 5 days, purified the GFP-positive cells by FACS, and injected the cells into the hearts of experimental MI rats at each of five sites at the border of the infarcted tissue. As a control, infarcted hearts were injected either with equal volumes and numbers of nonexposed (naive) BMMNCs or with saline. First, we revealed that donor-derived, exposed GFP-positive and SA- or ANF-positive cells were detected in abundance in the infarct border zone (Fig. 5B, a and d; 16.8% ± 2.1% of total cardiomyocytes in one field), but there were 15-fold fewer after injecting nonexposed GFP-positive cells (1.1% ± 0.4%). Hearts injected with exposed BMMNCs expressed SA-positive CMs, which also expressed connexin43 (Fig. 5B, a–c), and ANF (Fig. 5B, d–f). This indicated that transplanted BMMNCs formed gap junctions and intercalated disks and secreted CM-specific factor. Moreover, the assessment of cardiac function by echocardiography revealed that the hearts injected with exposed BMMNCs showed improved contractions of movement of the infarcted anterior walls and reduced left ventricular remodeling compared with the hearts injected with naive BMMNC or saline (Table 1). To exclude the possibilities of cell fusion in this model, we performed FISH staining with chromosome X- and Y-specific paint and revealed that educated BMMNCs (e-BMCs) implanted from male rats into female rats formed CM stained only with XY chromosome, not XXXY (Fig. 5C, a and b). This indicated that in vivo cardiac differentiation of BMMNCs was not induced by the fusion mechanism.

Nonhematopoietic Cells in the BM Are a Major Source of CM

Two candidates for the ability to regenerate myocardial tissue are HSCs and nonhematopoietic MSCs, as previously reported [1–4]. However, a recent report has indicated that the